Contrasted release of insoluble elements (Fe, Al, REE, Th, Pa) after dust deposition in seawater: a tank experiment approach

Matthieu Roy-Barman [1], Lorna Folio[1], Eric Douville[1], Nathalie Leblond[2], Frédéric Gazeau[3], Matthieu Bressac[3,4], Thibaut Wagener[5], Céline Ridame[6], Karine Desboeufs[7], Cécile Guieu[3]

[1] Université Paris-Saclay, CNRS, CEA, UVSQ, Laboratoire des Sciences du Climat et de l'Environnement, 91191, Gif-sur-Yvette, France

[2] Sorbonne Université, CNRS, Institut de la Mer de Villefranche, IMEV, F-06230 Villefranche-sur-Mer, France

[3] Sorbonne Université, CNRS, Laboratoire d'Océanographie de Villefranche, LOV, F-06230 Villefranche-sur-Mer, France

[4] Institute for Marine and Antarctic Studies, University of Tasmania, Hobart, Tasmania, Australia

[5] Aix Marseille Univ., Université de Toulon, CNRS, IRD, MIO UM 110, 13288, Marseille, France

[6] Sorbonne Université, LOCEAN, 4 Place Jussieu – 75252 Paris Cedex 05, France

[7] LISA, UMR7583, Université de Paris, Université Paris-Est-Créteil, Institut Pierre Simon Laplace (IPSL), Créteil, France

Correspondence to: Matthieu Roy-Barman (matthieu.roy-barman@lsce.ipsl.fr)

Abstract.

~~The release of~~ lithogenic elements ~~(which are often assumed to be insoluble)~~ such as Aluminum (Al), Iron (Fe), Rare Earth Elements (REE), Thorium (~~Th~~) and Protactinium (Pa)~~ by~~ Saharan dust reaching Mediterranean seawater ~~was studied~~ through tank experiments over 3 to 4 days under controlled conditions including control without dust addition ~~and~~ dust seeding under present and future climate conditions (+3 °C and -0.3 pH unit). Unfiltered surface seawater from 3 oligotrophic regions (Tyrrhenian Sea, Ionian Sea and Algerian Basin) were used. The maximum dissolution ~~fractions were~~ low for all seeding experiments: less than 0.3% for Fe, 1% for ^{232}Th and Al, about 2-5% for REE and less than 6% for Pa. Different behaviors were observed: dissolved Al increased until the end of the experiments, Fe did not dissolve significantly and Th and light REE were scavenged back on ~~the~~ particles after a fast initial release. The constant ^{230}Th/^{232}Th ratio during the scavenging phase suggests that there is little or no further dissolution after the initial Th release. Quite unexpectedly, comparison of present and future conditions indicates that changes in temperature and/or pH influence the release of thorium and REE in seawater, leading to ~~a~~ lower Th release and a higher light REE release under increased greenhouse conditions.

1 Introduction

The ocean biological productivity is strongly controlled by ~~inputs~~ of trace metals ~~like~~ iron (Fe), a limiting micronutrient for marine primary producers. Aeolian dust deposition over the ocean represents a significant Fe source for marine ~~surface~~ ecosystems (Duce and Tindale, 1991, Jickells et al., 2005). However, ~~the~~ aeolian Fe ~~flux is~~ difficult to ~~quantify precisely,~~ because ~~the~~ aeolian dust ~~deposition flux, the solubility of~~ Fe and ~~the~~ removal rate ~~of dissolved Fe~~ (by biotic and/or abiotic processes) are poorly constrained (Baker and Croot, 2010). To disentangle these processes, lithogenic tracers such as Aluminum (Al), Thorium (Th), Protactinium (Pa) and Rare Earth Elements (REE) that are not ~~involved (or not as much as Fe) in~~ biological processes are used to determine ~~the inputs of~~ lithogenic dust (Measures and Vink, 2000, Hsei et al., 2011, Greaves et al., 1999). This is based on the premise that ~~the content~~ of these lithogenic tracers ~~in surface waters~~ should be more or less proportional to their release rate by dissolution of aeolian dust as long as they are not actively removed by the biological activity. Moreover, thorium has one isotope (^{232}Th) derived from ~~the~~ lithogenic material ~~dissolution,~~ whereas ~~another one~~ (^{230}Th) is mostly produced in seawater by radioactive decay of conservative ^{234}U and ~~hence~~ can be used as a ~~chronometer of the~~ input and removal rate of ^{232}Th in ocean surface waters. A ~~key, but~~ poorly constrained parameter ~~used in~~ these ~~methods~~ is ~~the solubility of these~~ lithogenic ~~elements~~ (Anderson et al., 2016).

Here, we simulated Saharan dust deposition in surface Mediterranean seawater to determine the release of selected lithogenic tracers (Fe, Al, REE, Th, Pa). The main objective was to determine the solubility of these tracers, their dissolution kinetics and the possible influence of temperature, pH and biological activity. Dust deposition was simulated in tanks filled with unfiltered seawater (to ~~simulate~~ the impact of biological activity) ~~by adding at the beginning of the experiment~~ an amount of dust corresponding to strong Saharan dust deposition event over the Mediterranean Sea.

2 Methods

2.1 Experimental setup

A detailed description of the artificial dust addition experiments is given in Gazeau et al. (2020a, this issue). ~~In brief,~~ six experimental High Density PolyEthylene (HDPE) tanks (300 L each, with a conical base connected to a sediment trap~~) in which the irradiance spectrum and intensity can be finely controlled and in which future ocean acidification and warming conditions can be fully reproduced,~~ were installed in a temperature-controlled container during the PEACETIME cruise (doi: 10.17600/17000300). ~~This~~ cruise was conducted on board the R/V Pourquoi Pas? in the Mediterranean Sea during the late spring, a period characterized by strong stratification (Guieu et al., 2020, this issue). Three stations ~~covering~~ different *in situ* conditions ~~but~~ all characterized by oligotrophic conditions were chosen to conduct tank experiments ~~of 72 h (3 days)~~: stations TYR in the Tyrrhenian Sea, ION in the Ionian Sea and FAST in the Algerian basin (Fig. ES1, Guieu et al., 2020, this issue). The last experiment at station FAST was extended to four days. The experimental tanks were filled with unfiltered seawater from the continuous surface (5 m) pumping system upon arrival at stations TYR (17/05/2017) and ION (25/05/2017) and one day after arrival at station FAST (02/06/2017). Tanks C1 and C2 were unmodified control tanks, D1 and D2 were enriched with dust at the beginning of the experiment (3.6 g of dust per tank ~~or~~ 10 g m^{-2} ~~were~~ sprayed over each tank during ~20 minutes, ~~which correspond~~

~~to a~~ strong Saharan dust deposition event over the Mediterranean Sea – see section 4), ~~and~~ G1 and G2 were ~~warmed~~ (+3 °C), acidified (-0.3 pH unit) and enriched with dust ~~(same flux than in~~ D1 and D2). The atmosphere above tanks C1, C2, D1 and D2 was flushed with ambient air ~~and~~ tanks G1 and G2 were flushed with ~~air enriched~~ with CO_2 ~~(at 1000 ppm) in order~~ to prevent CO_2 degassing ~~from the acidified tanks. The originality of this device is that~~ the height of the tank (1.1 m) allows to take into account the settling of ~~the~~ particles and to analyze a series of parameters ~~both~~ in ~~the tank and at its base (sediment trap)~~.

Dust particles were derived from the fine fraction (< 20 μm) of a Saharan soil (Tunisia) ~~and~~ processed physically and chemically (including a treatment simulating the effect of cloud water and evapo-condensation) to produce an analogue of Saharan dust deposited over the Mediterranean Sea (see details in Guieu et al., 2010). The size spectrum of ~~these~~ dust ~~presents~~ a median diameter around 6.5 μm and a peak at ~ 10 μm similar to the one found in Mediterranean aerosols (Guieu et al., 2010). It is a mixture of quartz (~ 40 %) ~~and~~ calcite (~ 30 %), and different clay minerals (~ 25 %) (Desboeufs et al., 2014). ~~Chemically, it contains~~ 3.3 % ~~of~~ Al and 2.3 % ~~of~~ Fe. The detailed dust seeding procedure is ~~given in~~ Gazeau et al. (2020, this issue). ~~All tanks were sampled for dissolved Fe and Al before dust enrichment (t = 0 h) and then, 24 h and 72 h (TYR and ION) or 96 h (FAST) after dust enrichment.~~ Samples for Rare Earth Elements (REE), Th and Pa were ~~not~~ taken ~~at station TYR~~. At station ION, all tanks were sampled for Al, Fe and REE at t = 1, 24 and 72 h. At station FAST, tanks C1 and D1 were sampled for Al, Fe and REE at t = 0, 1, 6, 12, 24, 48, 72 and 96 h. ~~Tanks~~ G1 and G2 were sampled at t = 1, 48 and 96 h after dust enrichment.

At the end of each experiment, the particulate material that settled at the bottom of the tanks was recovered from the sediment traps and preserved by adding formaldehyde (~~final concentration~~ 5% ~~in~~ volume).

2.2 Analytical techniques

2.2.1 Dissolved Fe

Dissolved iron (DFe) concentrations were measured by flow injection with online preconcentration and chemiluminescence detection (Bonnet and Guieu, 2006; Guieu et al. 2018). An internal acidified seawater standard was measured daily to control the stability of ~~the~~ analysis. ~~During the analysis of the samples collected during the PEACETIME cruise,~~ the detection limit was 15 pM and the accuracy of the method was controlled by analyzing the SAFe S ~~(0.086 ± 0.010 nM (n = 3);~~ consensus value 0.093 ± 0.008 nmol·kg^{-1}, SAFe D1 ~~(0.64 ± 0.13 nmol·kg^{-1} (n = 19);~~ consensus value 0.67 ± 0.04 nM), GD ~~(1.04 ± 0.10 nM (n = 10);~~ consensus value 1.00 ± 0.10 nmol·kg^{-1}), and GSC ~~(1.37 ± 0.16 nmol·kg^{-1} (n = 4);~~ consensus value not available) seawater standards.

2.2.2 Dissolved Al

Determinations of dissolved aluminum (DAl) concentrations were conducted on board using the fluorometric method described by Hydes and Liss (1976). After filtration, samples were acidified to pH < 2 with double distilled concentrated HCl. After at least 24 h, the lumogallion reagent was added to the sample, which was then buffered to pH 5 with ammonium-acetate. The sample was then heated to 80°C for 1.5 h to accelerate the complex formation. The fluorescence of the sample was measured with a Jasco FP 2020 + spectrofluorometer (excitation wavelength 495 nm, emission wavelength 565 nm). The detection limit varied between 0.2 and 0.5 nM and the blank values between 0.9 and 1.7 nM for the different days of analysis. Based on the daily analysis of an internal reference standard ~~seawater~~, the overall ~~repeatability~~ of the method was 0.6 nM (standard deviation on a mean concentration of 53.5 nM, n = 25).

2.2.3 Dissolved REE, Th and Pa

Seawater was sampled from the tanks and filtered (pore size 0.45/0.2 µm; Sartobran®) within 1-2 h after sampling. acidified with trace metal grade HCl (NORMATOM®). Approximately 250 mL of filtered seawater was spiked with isotopes ^{150}Nd, ^{172}Yb, ^{229}Th and ^{233}Pa for isotope dilution measurements KMnO$_4$ and MnCl$_2$. REE, Th and Pa were pre-concentrated by co-precipitation raising pH to 8 through addition of concentrated NH$_3$. The MnO$_2$ precipitate was recovered by filtration onto a 25 mm cellulose ester filter, rinsed with MQ water and dissolved in a solution composed of 2 mL of 6N HCl and 10 µL of H$_2$O$_2$. REE, Th and Pa were separated using an AG1X8 ion exchange column (Gdaniec et al., 2018).

REE contents were measured at the LSCE using a quadrupole ICPMS (Xseries^{II}, Thermo Scientific©). Nd and Yb concentrations were directly determined by isotope dilution. Comparison of concentrations with the concentration determined by internal calibration (using In-Re internal standard) provided the yield of the chemical procedure (~70-100%). yields were used to estimate of the other REE, by assuming that yield is a linear function of the atomic number (Arraes-Mescoff et al., 1998).

Pa and Th analyses were performed using Inductively Coupled Plasma Mass Spectrometer (MCICP-MS, Neptune^{plus} ©) with a Secondary Electron Multiplier (SEM) and a Retarding Potential Quadrupole (RPQ) energy filter (Gdaniec et al., 2018).

Analyses of seawater used during the GEOTRACES intercalibration exercise (van der Fliert et al., 2012) showed agreements within a few percents with consensual values except La and Lu that were underestimated by 25% and 10% (Tab. ES1). Agreement within analytical uncertainties were obtained for ^{232}Th and age-corrected ^{230}Th concentrations. The very large uncertainties on ^{232}Th analyses of the GEOTRACES standard were due to its low ^{232}Th content (compared to Mediterranean seawater and the small sample volume used. 231Pa values are not reported because they correspond to the analysis series where yield and Blank problems were encountered for 231Pa analysis (see section 3.5).

2.2.4 Trapped particles

Samples were following the standard protocol developed at the national service "Cellule Piege" of the French INSU-CNRS (Guieu et al., 2005). Trapped particles were rinsed three times with ultrapure (MilliQ) water in order to remove salt and freeze-dried. Approximately 10 mg of were weighed and HNO$_3$/HF acid-digested using Suprapur reagents at 150 °C in PTFE vials. After complete evaporation, samples were diluted in 0.1 M HNO$_3$ and analyzed for Fe and Al concentrations by ICP-AES (JY 138"Ultrace", Jobin Yvon©). A fraction of the remaining solution was used to analyze REE, Th and Pa. Th and Pa, the solution was spiked with ^{229}Th and ^{233}Pa and treated through the same chemical process as the Mn precipitate used for the dissolved Pa and Th analysis. REE were analyzed directly on a quadrupole ICPMS (Xseries^{II}, Thermo Scientific©) using an internal calibration (Re).

3 Results

3.1 Dissolved Fe

Over the course of the three experiments, DFe concentrations in control tanks were in the range of 0.7-2.5 nM (Tab. ES2, Fig. 1) in good agreement with DFe measured during the cruise (TYR: 1.47 ± 0.30 nM; ION: 1.41 ± 0.19 nM; FAST: 1.71 ± 0.35 nM, Bressac et al., in prep.) and with surface concentrations observed in the Mediterranean Sea during the stratification period (Bonnet and Guieu 2006; Gerringa et al., 2017; Wagener et al., 2008). For the TYR experiment, there was no clear difference between controls (C1 and C2) and dust amended tanks (D1, D2, G1 and G2) that would indicate significant release from dust.

5

For the ION experiment, ~~the~~ concentrations measured in G1 were much higher than in ~~the~~ other tanks and most likely ~~highlighted a~~ contamination ~~issue. For the FAST experiment,~~ DFe concentrations were lower in control tanks than in dust amended tanks. However, ~~during this experiment,~~ high variability between duplicates suggest possible contamination ~~issues~~ during sampling or sample processing.

5

3.2 Dissolved Al

The Al concentrations in control tanks ~~varied between stations:~~ ~ 50 nM at TYR, ~ 75 nM at ION and ~20-25 nM at FAST (Tab. ES2, Fig. 1). ~~All~~ these values are within the range of concentrations observed in Mediterranean surface waters (Rolison et al., 2015). ~~At all three stations, Al concentrations measured before dust addition (t = 0 h)~~
10 ~~were similar in all tanks.~~ After dust addition, Al concentrations ~~steadily~~ increased in ~~tanks~~ D and G ~~to reach~~ final concentrations 50-100 nM higher than in control tanks ~~with no systematic~~ differences between D and G treatments. The ~~concentration~~ increase at FAST (72-80 nM) was ~~higher~~ than at TYR and ION (52-68 nM), due to a longer experiment ~~at FAST.~~

15 ## 3.3 Dissolved Rare Earth Elements

The REE concentrations measured in control tanks at stations ION and FAST (Tab. ES3, Fig. 2) compares well with values reported in the Mediterranean Sea (Censi et al., 2004, Tachikawa et al., 2008). In control tanks at both ION and FAST, ~~there was~~ a slight increase in concentrations during the course of the experiments ~~suggesting~~ some contamination from the tank or the environment of the experiment. ~~However, this increase remained limited~~ (i.e. ≃
20 +15-40% for dissolved Nd, ≃ +5-10% for dissolved Yb) compared to changes in concentrations observed in the dust amended tanks. For both D and G, there was a sharp increase in the concentrations of all REE (~~i.e.~~ ≃ +400% for dissolved Nd, ≃ +100% for dissolved Yb), followed by a slow ~~decrease.~~ The ~~sharp~~ increase can be observed by comparing the REE concentrations at t= 0 (before dust seeding) and t = 1h during the D1 experiment at FAST. For the other experiments (including the ION tanks), the comparison the D or G concentrations at t=1h after dust seeding,
25 with the concentrations recorded in the C series (no seeding) also highlight a sharp increase of the REE concentrations. ~~The decrease was steeper for light Rare Earth elements (LREE, e.g. Nd for which the concentration decrease was visible as early as t = +6 h) than for heavy Rare Earth elements (HREE, e.g. Yb for which the concentration remained relatively constant after t = +1 h).~~ The only exception in these regular trends was observed at FAST for tank D2, where no increase in REE concentrations was observed after dust addition (t = +1 h). As this most likely resulted from a
30 technical issue during sampling (perhaps bottle labelling), we will consider this value as an outlier. In general, ~~REE concentrations~~ at a given time and site ~~were higher~~ (LREE) ~~or equivalent~~ (HREE) in the warmer and acidified tanks (G) as compared to ambient environmental conditions (D).

3.4 Dissolved Thorium isotopes

35 ~~Most~~ ^{232}Th concentrations in control tanks ~~were about 1 pM both~~ at FAST and ION (Tab. ES3, Fig. 3), in agreement with surface water concentrations in the Mediterranean Sea (Gdaniec et al., 2018). ~~Only one high~~ ^{232}Th concentration was measured in tank C1 at station FAST 12 h after ~~dust addition~~ (~10 pM). Since the ~~following value measured in~~ this tank (t = +24 h) was in the expected range (~1 pM), this extreme value likely resulted from a sample contamination, rather than a contamination of the tank itself. Slightly higher LREE concentrations for this sample, ~~as~~
40 compared to ~~levels measured~~ at the other time points supported ~~this~~ sample contamination hypothesis. REE have a longer residence time in seawater than Th and ~~therefore, they~~ are ~~theoretically~~ less sensitive to contamination from lithogenic material. As for REE, there was a sharp increase of ^{232}Th concentrations after dust addition at both ION and FAST. ~~At FAST,~~ concentrations were higher in tank D1 ~~at t = +12 h and t = +24 h than at t = 1 h.~~ However, as described

above for tank C1 at station FAST and for the sampling time t = +12 h, we consider that these high values can be attributed to sample contamination during sampling. Therefore, we will not consider further these two samples (Fig. 3).

5   After the rapid ^{232}Th increase for the D and G treatments at FAST and ION, there was a systematic decrease of the ^{232}Th concentration. In contrast to REE, ^{232}Th concentrations were higher in D tanks compared to G tanks.

The variations of ^{230}Th concentrations with time and between treatments were similar than what described for ^{232}Th concentrations. However, significant variations of the ^{230}Th/^{232}Th ratio were observed (Tab. ES3, Fig. 3, Fig. 10 ES.3). The highest ratios (^{230}Th/^{232}Th ≥ 1 × 10^{-6} mol/mol) were measured in controls, whereas lower ratios (^{230}Th/^{232}Th ≤ 1 × 10^{-6} mol/mol) were found in D and G tanks.

3.5 Dissolved Protactinium

15   Due to analytical problems (low yield and large blanks) largely due to the small volumes available and low Pa content in the Mediterranean surface water, only Pa results obtained at FAST for tanks C1 and D1 will be presented. The mean ^{231}Pa concentrations at FAST were not different within uncertainties in the C1 (2.5 ± 0.2 aM, with 1 aM = 10^{-18} M) and D1 (2.4 ± 0.2 aM) treatments (Tab. ES3, Fig. 4). Despite the small volumes of seawater analyzed, these concentrations agree within uncertainties, with the Pa concentrations available in surface western Mediterranean Sea 20   (Gdaniec et al., 2017). Due to relatively large uncertainties on individual data, no systematic temporal trend is depictable.

3.6 Trapped material

25   The material collected in the traps contained 2.6% of Fe and 4.8% of Al (Tab. ES4). This is higher than the initial dust composition (2.3% of Fe and 3.3% of Al), due to preferential dissolution of highly soluble calcium carbonate or possibly calcium hydrogen carbonate formed during the simulation of dust processing in clouds (see section 2.1., Desboeufs et al., 2014). The lower Ca (14.2%) content in the trapped material compared to the initial dust (16.54%) suggests ~ 15% of calcium carbonate dissolution (~4.5% of the total mass as carbonates represent 30   ~30% of the dust). REE concentrations in the sediment trap are close to concentrations in the average upper continental crust (Taylor and McLennan, 1995), yielding flat REE patterns (Tab. ES5, Fig. ES2). The particulate ^{232}Th concentrations are within a range of 70 ± 5% of the upper continental crust concentration. The ^{230}Th concentrations correspond roughly to secular equilibrium for a U/Th ratio of 0.40, in agreement with the range observed in the average continental crust. The ^{231}Pa concentrations correspond to secular equilibrium for a U/Th ratio 35   of 0.34, slightly below the ratio calculated with ^{230}Th but still in agreement with the crustal range and Saharan aerosols (Pham et al., 2005).

4 Discussion

The concentration changes observed during the experiments resulted from a net balance between the release 40   of chemical elements by the dissolution of the dust and removal of these elements on the particles by scavenging or active (biological) uptake. For an element like Fe, the scavenging efficiency largely depends on Fe stabilization in the

7

dissolved phase by Fe-binding molecules (Witter et al. 2000). As the dust concentration was high, Fe readsorption on the dust could have been particularly high (Wagener et al., 2010). Dust inputs over the Mediterranean Sea are very irregular (Loÿe-Pilot & Martin, 1996). The dust quantity used for the seeding (10 g of total dust/m^2 with an Al content of 4%) corresponds to the highest dust pulses observed over the Mediterranean Sea during one rain event (e.g. Ternon et al., 2010) and represents 30-100% of the dust quantity deposited yearly over the Mediterranean Sea (Guieu et al., 2010b). Hence, the PEACETIME experiments gives an idea of the yearly release of insoluble elements in the Mediterranean surface waters. To use the PEACETIME results in ocean basin with lower dust inputs, we will also evaluate the percentage of dissolution of these elements from the dust by dividing the observed concentration changes in the dissolved phase by the concentration of particulate element carried by dust in the tank (see equation 1 below).

4.1 Solubility of tracers

The percentage of dissolution of the different elements was calculated as the maximum release of the considered dissolved element during the experiments (largest difference in concentrations between D or G tanks and control tanks) divided by the amount of particulate tracers per volume of seawater introduced in the tanks by dust addition (Tab. 1) following the equation:

$$f_{dissol\_conc} = \frac{CONC_{max} - CONC_{init}}{CONC_{dust} \times m/V} \times 100 \qquad (1)$$

.

where $CONC_{dust}$ is the concentration in the original dust (expressed in mol of insoluble element/g of dust), m represents the mass of dust added to the tank and V represents the volume of seawater in the tank. Direct analysis of the original dust was used for total Fe and Al (Guieu et al., 2010). For REE, Th and Pa, we used the average concentrations of particles collected in the traps decreased by 15% to account for the carbonate dissolution (see section 3.6). The mass of dust deposited in each tank (3.6 g) is noted m and V is the volume of the tank (300 L). During the course of the experiments, the dust loss by sedimentation ranged from 28 to 65% likely depending on the intensity of aggregation in each tank (as previously observed by Bressac et al., 2011). However, it did not seemed to impact the estimation of the percentage of dissolution. For example, at the ION station, while a large difference was observed between the amount of Al collected in the sediment traps of D1 and D2 (75% and 33% of the Al introduced when seeding were recovered in the traps, respectively, so that only 25% and 67% of the initial particulate remained in suspension at the end of the experiment), the percentages of dissolution were identical in D1 and D2 for all the studied elements (Fig 1-3, Table 1).

We suggested in section 3 that the DFe concentrations can be biased by contaminations during the experiments. Nevertheless, we can put an upper limit to Fe dissolution by assuming that the highest DFe concentrations measured during the experiments truly represents Fe dust release. The highest DFe (10 nM) was measured at station FAST in the dust amended tank D1 at t = 72 h. Considering that when seeding the dust at the seawater surface of each tank, 30 μM of particulate Fe ($CONC_{dust}$ for Fe) were added, it follows that Fe dissolution extent is at most ~ 0.3%. This result is in good agreement with the percentage of dissolution of Fe obtained using the same dust and device with filtered seawater from coastal Northwestern Mediterranean Sea under abiotic conditions in May (Bressac and Guieu, 2013, Louis et al., 2018).

For [231]Pa, we were not able to detect a significant difference between C1 and D1 at FAST. However, we can set an upper limit on Pa dissolution. Based on trap analyses (Tab. ES5), we estimate that [231]Pa$_{dust}$ ×m/V= 0.04 fM. Given the analytical uncertainties on dissolved [231]Pa analysis (Fig. 4), $CONC_{max}$ - $CONC_{init}$ is certainly below 0.002 fM. Hence, the percentage of dissolution of [231]Pa is below 5%. As expected for these poorly soluble elements, the

maximum percentages of dissolution were low for all stations: less than 0.3% for Fe, 1% for [232]Th and Al (although their dissolution kinetics do not have the same patterns) and about 2-5% for REE.

Looking more into details, it appeared that Al dissolution was slightly higher at FAST compared to ION, but identical in D and G treatments. The contrasting behaviors of Al that progressively dissolved during the experiments compared to Fe that did not dissolve significantly may be due to their respective solubility limit. The Al concentrations (~50 - 100 nM) during the experiments were much lower than the dissolved Al concentration in seawater at equilibrium with Al hydroxides which is at the micromolar level (Savenko and Savenko, 2011). By contrast, dissolved Fe concentrations during the experiments were close or above the theoretical solubility of Fe hydroxides in seawater (Millero, 1998) due to the presence of Fe-binding ligands that keep Fe in solution (Wagener et al., 2008). For Al (as well as for Fe), there was no sample analysis at t = 1 h (just after dust addition), so it was not possible to detect a putative early dissolution as observed for REE and Th (see below).

For Th, the 2 samples considered as contaminated in section 3.4 are not considered hereafter (Fig. 3). Moreover, taking these two samples into account or not would not significantly affect the main conclusions of this study regarding Th. In contrast to Al, both Th and REE were released rapidly after dust addition, similarly to phosphate and nitrate (Gazeau et al., 2020, this issue). Fortuitously or not, it appears that more Th and Dissolved Inorganic Phosphorus (DIP) were released at FAST than at ION. Among the differences between ION and FAST, we note that FAST has a higher biomass than ION (although this is most visible at the end of the experiment, whereas Th release occurs during the first hour) and a lower alkalinity (Gazeau et al., 2020). However, this relationship with biomass does not hold if we compare the D and the G experiments. For both FAST and ION, there is more Th dissolution in the D tank compared to G tank (Fig. 2), whereas more biomass increase was observed under greenhouse conditions compared to normal conditions (Gazeau et al., 2020, this issue). The higher temperature imposed in tanks G induced a higher concentration of Transparent Exopolymeric Particles (TEP; Gazeau et al., in prep). The high affinity of Th for TEP (Santchi et al., 2004) combined with the aggregation of TEP on particles could limit the presence of Th in the G treatment as compared to D. At present, we must recognize that it is not possible to determine unambiguously the parameter(s) controlling the low percentage of Th release.

For REE, percentages of dissolution were relatively similar at FAST and ION, but unlike Th, slightly lower LREE dissolution fractions occurred under ambient environmental conditions (D, 1.9% for La) than under future conditions (G, 2.3% for La). The REE percentage of dissolution increased regularly from La (~2%) to Dy (~5%) and then decreased towards Lu (~3%) (Fig. 5a). It closely mimics the solubility pattern obtained by leaching Saharan aerosols with filtered seawater (Greaves et al., 1994). In this latter study, the mid-REE maximum of percentage of dissolution was attributed to Fe oxyhydroxides (Haley et al., 2004), with Fe oxyhydroxides being the main phase releasing REE, but Fe solubility was not measured. Here, we show that the percentage of REE dissolution exceeds by far the percentage of Fe release, possibly due to the high REE content of Fe oxyhydroxides (Haley et al., 2004).

An unexpected result of the PEACETIME experiments is the contrasting dissolution kinetics of Al relative to Th and REE. Th and REE are (at least partly) carried by specific REE and Th rich phases (Marchandise et al., 2014), that may account for the decoupling with Al. Alternatively, the fast dissolution of calcium carbonate or calcium hydrogen carbonate formed during the cloud simulation step could account for REE and Th release (see sections 3.6 and 4.3.).

The soluble fraction of Mediterranean aerosols was also evaluated by leaching aerosols collected during the PEACETIME cruise in ultrapure water for 30 min (Fu et al., 2020, this issue). There was a relatively good agreement for Nd between these aerosol leaching experiments (median percentage of Nd dissolution = 6%) and the percentage of Nd dissolution observed in our tank experiments (3%). These low values are also consistent with former estimates based on Saharan aerosol leaching in distilled water (1-3 %; Greaves et al., 1994). In contrast, aerosol leaching during PEACETIME suggested much larger Al and Fe solubilities (around 20%) than those observed during our dust addition experiments. These highest percentages of dissolution reflect mainly the anthropogenic influence in the aerosol samples collected during the cruise that were characterized by mixing between Saharan and polluted air masses (Fu et al., 2020, this issue). Indeed, anthropogenic metals are largely more soluble than metals issued from desert dust (Desboeufs et al., 2005). However, the solubility values obtained in our dust addition experiments for Al and Fe are in agreement with the values found in ultrapure water for the same amended dust (Aghnatios et al., 2014), for other analogs of Saharan dust (Desboeufs et al., 2001; Paris et al., 2011) or for dust collected over Sahara (Paris et al., 2010). We conclude that the percentages of particulate Al and Fe obtained in our experiments are representative of pure Saharan dust inputs.

4.2 Removal of dissolved tracers

During the experiments, biological uptake or scavenging onto particulate matter may have biased the estimation of percentage dissolution of insoluble elements. Fe and Al are well known for being incorporated during biological processes: Fe as a micronutrient (e.g. Twinings et al., 2015) and Al by substitution to Si in diatom frustules (Gehlen et al., 2002). Could the lack of increase of dissolved Fe be due to biological uptake? We estimate this uptake with the Chlorophyll a (Chl$a$) increase observed during the course of the experiments (~ 0.5 $\mu g \cdot L^{-1}$), a C/Chla ratio of ~ 50 mg C/mg Chl$a$ and a Fe/C ratio ranging from 10 μmol/mol to 100 μmol/mol (Twinings et al., 2015). It yields that the biological activity should have taken up at most 0.25 nM of Fe, which is an order of magnitude less than the dissolved Fe measured during the course experiments. Therefore, any significant Fe release by dust would not have been masked by biological uptake. We also estimated if the development of diatoms during the experiment can remove a significant fraction of Al from the solution. Using the biogenic silica flux measured in the sediment traps (~ 10-40 mg$\cdot$m$^{-2}\cdot$d^{-1}) and an Al/Si ratio in diatom frustules of 0.008 (maximal value in Gehlen et al., 2002, to maximize the effect), we calculated that diatoms could have consumed as much as 6-18 nM Si. This represents a small but not completely negligible fraction of the Al released by the dust.

As REE and Th are not known to be involved in biological cycles, their decreasing concentrations during the course of the experiments suggests that they may be removed by scavenging onto particles due to abiotic processes. We define the percentage of scavenging as follow:

$$f_{scav} = \frac{CONC_{max} - CONC_{min}}{CONC_{max}} \times 100 \qquad (2)$$

Th appeared to be the element most sensitive to scavenging (43-44% at ION and 65-70% at FAST). The REE scavenging was less extensive and decreased from LREE (15-37%) to HREE (1-13%; Fig. 5b). This reduced scavenging of HREE compared to LREE is consistent with the stronger complexation of HREE by carbonate ions that stabilize them in seawater (Tachikawa et al., 1999) and was already observed during equilibrium experiments between seawater and synthetic minerals (Koeppenkastrop and Eric, 1992). In terms of REE fractionation, the net effect of preferential Mid-Rare Earth Elements (MREE) release (from particles enriched in MREE) and the preferential

scavenging of LREE ~~compared to HREE~~ results in a shale-normalized REE pattern with ~~a reduced~~ depletion of LREE ~~compared to HREE, but~~ a flat pattern from MREE to HREE (Fig. ES 2).

~~For both Th and LREE,~~ the scavenged fraction ~~is larger~~ at FAST than at ION. At each station, similar ~~scavenging percentages~~ were obtained from D and G ~~experiments. When discussing scavenging, it must be kept in~~ ~~mind that the large amount of dust initially introduced in the tanks, yielded an unusually high particle content in~~ ~~seawater.~~ Considering that 3.6 g of dust were introduced in 300 L of seawater, ~~that~~ <mark>~50%</mark> of the fast-sinking large particles (Bressac et al., 2011) sedimented to the bottom trap ~~and that~~ 15% of carbonate dissolution occurred (see section 3.1, Desboeufs et al., 2014), the average dust concentration remaining in suspension in the tank was <mark>~ 5000</mark> $\mu g \cdot L^{-1}$. This ~~was~~ several orders of magnitude higher than typical particulate matter concentrations in seawater (1-100 $\mu g \cdot L^{-1}$, Lal, 1977), not impacted by a recent dust deposition event. At these high particulate matter concentrations, it is ~~expected~~ that scavenging of insoluble elements ~~onto~~ suspended dust ~~can occur.~~ Adsorption experiments of a radioactive Ce tracer on deep sea clays showed a decrease of 30 % ~~of the~~ dissolved Ce over a few days (Li et al., 1984), ~~which is grossly~~ comparable to the results presented here. The~~se~~ experiments on deep sea clays were carried in abiotic conditions, raising the possibility that adsorption observed during the tank experiments were, at least in part, due to abiotic processes on the dust. However, ~~as~~ the dust used during ION and FAST ~~were strictly similar~~, it is likely that ~~larger and faster~~ scavenging at FAST compared to ION was due to ~~the~~ higher biological activity at FAST ~~compared to~~ ~~ION~~ (Gazeau et al., 2020a, this issue). ~~Among biologically produced molecules,~~ <mark>Th has a high affinity for TEP</mark> <mark>(Santschi et al., 2006). However, there not a marked difference in TEP content at ION compared to FAST (Gazeau et</mark> <mark>al., 2020b, this issue.</mark> We note that ~~very high dust content and~~ adsorption rates were reached because all the dust was deposited instantaneously at the beginning of the experiment. Deposition of the same amount of dust over longer periods (weeks, months) as it occurs in less dusty environment ~~than the Mediterranean Sea~~, would certainly result in less readsorption (but likely similar ~~percentages of~~ dissolution).

4.3 Thorium isotopes

When reversible processes affecting Th occur, the $^{230}Th/^{232}Th$ ratio is a good tracer of the Th fluxes (Roy-Barman et al., 2002). The rationale is that the $^{230}Th/^{232}Th$ ratio in <mark>initial</mark> seawater ($^{230}Th/^{232}Th \approx 15 \times 10^{-6}$, Gdaniec et al., 2018) is higher than the $^{230}Th/^{232}Th$ ratio in the dust ($^{230}Th/^{232}Th \approx 3\text{-}6 \times 10^{-6}$; Pham et al., 2005; Roy-Barman et al., 2009). Hence, as dust releases ~~dissolved~~ Th in the tanks, the seawater $^{230}Th/^{232}Th$ ratio decreases. Conversely, when dissolved Th is scavenged on the particles, both isotopes behave similarly and the isotopic ratio of the seawater inside the tank remains constant. Hence the $^{230}Th/^{232}Th$ ratio ~~of the~~ seawater ~~keeps track of the~~ Th released from dust even ~~if~~ ~~some~~ readsorption occurs. ~~As there is far more~~ Th in the dust than in ~~the initial~~ seawater, the $^{230}Th/^{232}Th$ ratio ~~of the~~ ~~particulate~~ matter remains virtually constant even if seawater-derived Th ~~sorbs on the particles.~~

~~These changes in concentration and isotopic ratios are best illustrated by plotting the~~ $^{230}Th/^{232}Th$ ~~ratio as a~~ ~~function of 1/^{232}Th (Fig. 6).~~ On ~~this~~ diagram, the theoretical evolution of the filtered seawater samples with time should be: (1) for simple dissolution, filtered seawater samples lie on a straight line between labile marine particles and seawater blanks; (2) if readsorption occurs, the filtered seawater samples will be shifted horizontally toward the right; (3) for rapid reversible equilibrium between seawater and particles, filtered seawater samples should lie on a straight vertical line (Arraes-Mescoff et al., 2001). For the ION experiments, C samples and the samples of the D and G treatments at t = 1 h plot on an oblique straight line, suggesting that the initial increase in seawater Th concentration results from the simple dissolution of marine particles. On this diagram, the intercept at $1/^{232}Th = 0$ represents the

^{230}Th/^{232}Th of the dissolving particulate matter. It appears that this ratio is about $(8.5 \pm 0.8) \times 10^{-6}$ mol/mol, significantly above the ratio measured on the trapped particles ($\sim (6 \pm 0.5) \times 10^{-6}$) or estimated for Saharan dust (Pham et al., 2005, Roy-Barman et al., 2009). It suggests that there might be a preferential release of ^{230}Th compared to ^{232}Th due to the combined effect of the recoil of two alpha decays ~~between~~ ^{238}U ~~and~~ ^{230}Th and the variable U/Th ratio observed among the phases carrying U and Th (Bourne et al., 2012, Bosia et al., 2018, Marchandise et al., 2014). Alternatively, the dissolution of the carbonates from the dusts can release significant amounts of ^{232}Th~~.~~ ~~For example, the~~ ^{232}Th ~~content of~~ travertine and pedogenic carbonates ~~found in~~ the Western Sahara ~~ranges~~ from 0.5 to 12 ppm (Szabo et al., 1995, Candy et al., 2004, Weisrock et al., 2008). ~~Taking~~ 2 ppm ~~as mean value~~ and considering that carbonate dissolution represents 4.5 % of the dust mass (see section 3.6), ~~it corresponds to a release of 1400 pmol in 300L of seawater potentially yielding~~ an increase of 5 pM~~,~~ ~~in gross agreement with~~ observations (Fig. 3). While pedogenic calcretes contain sufficient amounts of ^{232}Th and REE to account for the changes of Th and REE concentrations observed during the ~~Peacetime~~ experiments (Prudencio et al., 2011), the ^{230}Th/^{232}Th ratio of these carbonates is generally low (^{230}Th/^{232}Th = 2-5$\times 10^{-6}$, Candy et al., 2004), so that it cannot account for the higher ^{230}Th/^{232}Th ratio ($\sim 8 \times 10^{-6}$) ~~of the Th released during the PEACETIME~~ experiments (Fig. 6).

Samples from the D and G treatments (t = 1 h to 72 h) plot on a horizontal line (with little change of the ^{230}Th/^{232}Th ratio) confirming that simple reabsorption occurs after the initial dissolution (with little or no release of particulate Th after the initial dissolution observed at t = 1 h).

A simple mass balance gives the fraction of dissolved ^{232}Th in seawater ~~coming~~ from the dissolution of particulate Th (Roy-Barman et al., 2002):

$$f_{litho} = \frac{\left(\frac{230Th}{232Th}\right)_{D\ or\ G} - \left(\frac{230Th}{232Th}\right)_{C}}{\left(\frac{230Th}{232Th}\right)_{litho} - \left(\frac{230Th}{232Th}\right)_{C}} \tag{3}$$

Knowing f_{litho}, we can determine f_{dissol_isot}, the dissolution fraction based on the isotopic data:

$$f_{diss\_isot} = \frac{CONC_{init}\left(\frac{f_{litho}}{1 - f_{litho}}\right)}{CONC_{dust} m/V} \tag{4}$$

This estimate is independent on ~~the concentration data~~ that may be biased by readsorption. We evaluate f_{dissol_isot} based on average ratios ~~of the C series~~ for original seawater and the average ratio of the last samples of the D and G treatments~~,~~ to ~~integrate~~ dissolution over the course of the whole experiment (Tab. ES3). For the particulate ratio, we tentatively used a ratio of 8.5$\times 10^{-6}$ mol/mol (value best defined by the y-axis value for $1/^{232}$Th = 0 of the dissolution and scavenging trends at ION, Fig. 5).

The resulting average f_{dissol_isot} are below 3% for FAST D~~, FAST G,~~ ION D and ~~ION~~ G, confirming the low solubility of Th (Tab. 1). While we recognize that for FAST, the large data scatter~~ing~~ results in large uncertainties on the interpretation of the results, all the results obtained during PEACETIME ~~argue for~~ a low ~~solubility of Th.~~

4.4 implication for dust deposition estimation

The ^{230}Th/^{232}Th ratio in the surface ocean is proposed as a tracer to monitor the dust inputs and the release of trace metals at the ocean surface (Hsieh et al., 2012). The rational is that, neglecting lateral transport, ^{232}Th is provided by dust dissolution whereas ^{230}Th comes mostly from the *in situ* decay of ^{234}U and can be used as a chronometer for ^{232}Th dissolution. If the solubility of ^{232}Th from dust is known, it is possible to calculate the dust flux required to account for the ^{230}Th/^{232}Th ratio of the surface waters. Until now, the ^{232}Th solubility from dust was poorly constrained. By adjusting the percentage of lithogenic ^{232}Th dissolution to match the ^{230}Th/^{232}Th ratio in the surface water of the Atlantic Ocean and using dust fluxes from a global dust deposition model, it was proposed that the fraction of lithogenic ^{232}Th dissolution grossly range between 1 and 5% in high dust flux areas such as the East equatorial Atlantic and up to 10-16 % in areas of low dust deposition such as the South Atlantic (Hsieh et al., 2012). Estimated ^{232}Th percentage of dissolution at the Bermuda Atlantic Time-series Study (BATS) ranged from ~1 to 68% and increased with the assumed aerosol dissolution depth range (Hayes et al., 2017). Alternatively, the soluble fraction of ^{232}Th in atmospheric dust was estimated by leaching particles with deionized water or dilute acetic acid, but the 2 types of leaching provided no consensus results (Anderson et al., 2017).

The present work indicates a low ^{232}Th fractional solubility (percentage of dissolution ~1%) for the material used for the tank experiments. It is lower but quantitatively consistent with the low solubility (percentage of dissolution ~3-5%) of lithogenic Th derived from a gross western Mediterranean budget of Th isotopes in which Th inputs are dominated by ocean margins (Roy-Barman et al., 2002) and with the low overall fractional solubility of Th (~ 4-8%) from Saharan aerosols estimated by leaching with ammonium acetate solution at pH 4.7 (Baker et al., 2020). Keeping in mind the limitation of our study (limited time duration, very high particle concentration promoting re-adsorption), these results argue for a low ^{232}Th solubility. It suggests that the high Th solubility derived by balancing the lithogenic Th input by dust with the scavenging on settling particles could be biased by advective inputs (Hayes et al., 2017). Hence, deducing dust inputs from the ^{230}Th/^{232}Th ratio of surface waters (Hsieh et al., 2012) requires first to consider ocean areas where the water residence time relative to circulation significantly exceeds the Th residence time relative to scavenging (e.g.: part of the south Pacific gyre where the horizontal dissolved ^{232}Th gradient tend to vanish (Pavia et al., 2020)).

One aim of these ^{230}Th-^{232}Th based estimates of the dust deposition is to evaluate the supply of dissolved Fe at the ocean surface. To circumvent the difficulty of determining absolute percentages of dissolutions of trace metal from dusts, relative fractional solubility of Fe relative to Th (the ratio of the percentage of Fe dissolution to the percentage of Th dissolution from the dust) is used as a more robust model parameter. It is often assumed that the percentages of dissolution of Fe and Th are identical yielding a Fe/Th ratio released by dust dissolution of the order of 20000 mol/mol (Hayes et al., 2017, Pavia et al., 2020). Aerosol leaching experiments suggest a preferential release of Th compared to Fe with a Fe/Th ratio released by dust dissolution of the order of 10000 mol/mol (Baker et al., 2020). Keeping in mind potential bias due to the different dissolution kinetics, a salient result of the PEACETIME tank experiments is the much lower (by a factor ~100) percentage of dissolution of Fe relative to Th, yielding an upper limit for the released Fe/Th ratio below 200-1500 mol/mol (Tab. ES5).

5 Conclusion

The PEACETIME tank experiments ~~have allowed to quantify~~ the particulate-dissolved exchanges of Al, Fe, REE, Pa and Th following Saharan dust addition to surface seawater ~~in~~ three basins of the Mediterranean Sea under present and future climate conditions. ~~In particular, we report here the first estimates of thorium and protactinium.~~ We highlight differences ~~of percentages~~ and kinetics of dissolution as well as scavenging among the lithogenic tracers: ~~under~~ the experimental conditions, Fe dissolution was ~~much more buffered~~ than the dissolution of Th, REE or Al. As a consequence, assuming ~~a congruent~~ dissolution ~~of~~ lithogenic tracers to evaluate Fe fluxes is ~~probably~~ generally not appropriate. Using relative solubility, might be also biased by the different dissolution and scavenging kinetics characterizing each tracer. Quite unexpectedly, comparison of present and future conditions indicates that changes in temperature (+3 °C) and/or pH (-0.3 pH unit) influence the release of ~~thorium~~ and REE in seawater, leading to a lower Th release and a higher light REE release under increased greenhouse conditions. Using Th isotopes, we show that Th was released within the first hour of the experiment and that no subsequent Th release occurs during the following days. This observation, associated to the low percentage (1%) of Th dissolution from dust puts strong constraints on the use of Th isotopes as a tracer of dust inputs in surface waters. ~~If generalizable to all dust inputs over the ocean,~~ and highlights the importance of advection as a source of [232]Th is the open ocean.

The implications of these experiments are not limited to constrain aeolian inputs to the surface ocean. They also contribute to a better understanding of the strong contrast in vertical profiles and zonal distribution of insoluble elements in the Mediterranean Sea. In this region, dissolved Al increases from surface to deep waters and also from the ~~deep~~ western ~~basin~~ to the ~~deep~~ eastern basin (Rolison et al., 2015), ~~whereas dissolved~~ Fe and [232]Th profiles often present surface concentration maxima and no systematic concentration gradient between the ~~deep~~ western and ~~deep~~ eastern basins (Gerringa et al., 2017; Gdaniec et al., 2018). While the Al and Th ~~percentages of dissolution from dust were comparable during~~ the tank experiments, kinetics were different: Th ~~strongly scavenged~~ after the initial release, ~~whereas~~ Al ~~kept dissolving all time long.~~ It highlights the highly particle-reactive character of Th compared to Al. Hence [232]Th, cannot accumulate along the Mediterranean deep circulation and does not exhibit a zonal gradient ~~like~~ Al ~~does~~.

Competing interests

The authors declare that they have no conflict of interest, no competing financial interests.

Acknowledgements

References

Anderson, R. F., Fleisher, M. Q., Robinson, L., Edwards, R. L., Hoff, J. A., Moran, S. B., Rutgers van der Loeff, M. M., Thomas, A. L., Roy-Barman, M., and Francois, R.: GEOTRACES intercalibration of ^{230}Th, ^{232}Th, ^{231}Pa, and prospects for ^{10}Be, Limnol. Oceanogr.: Methods, 10, 179-213, 2012.

Anderson, R. F., Cheng, H., Edwards, R. L., Fleisher, M. Q., Hayes, C. T., Huang, K. F., ... & Lu, Y.: How well can we quantify dust deposition to the ocean?. Philosophical Transactions of the Royal Society A: Mathematical, Physical and Engineering Sciences 374, 20150285, 2016.

Aghnatios, C., Losno, R., and Dulac, F.: A fine fraction of soil used as an aerosol analogue during the DUNE experiment: sequential solubility in water, decreasing pH step-by-step, Biogeosciences, 11, 4627–4633, https://doi.org/10.5194/bg-11-4627-2014, 2014.

Arraes-Mescoff, R., Roy-Barman, M., Coppola, L., Souhaut, M., Tachikawa, K., Jeandel, C., ... & Yoro, C.: The behavior of Al, Mn, Ba, Sr, REE and Th isotopes during in vitro degradation of large marine particles. Mar. Chem. 73, 1-19, 2001.

Azetsu-Scott, K., & Niven, S. E.: The role of transparent exopolymer particles (TEP) in the transport of 234Th in coastal water during a spring bloom. *Continental shelf research 25*, 1133-1141, 2005.

Baker, A. R., & Croot, P. L.: Atmospheric and marine controls on aerosol iron solubility in seawater. *Marine Chemistry*, *120*(1-4), 4-13, 2010.

Baker, A. R., Li, M., & Chance, R.: Trace metal fractional solubility in size-segregated aerosols from the tropical eastern Atlantic Ocean. *Global Biogeochemical Cycles*, *34*(6), e2019GB006510, 2020.

Bosia, C., Chabaux, F., Pelt, E., Cogez, A., Stille, P., Deloule, E., & France-Lanord, C.: U-series disequilibria in minerals from Gandak River sediments (Himalaya). Chemical Geology, 477, 22-34, 2018.

Bonnet, S., & Guieu, C.. Atmospheric forcing on the annual iron cycle in the western Mediterranean Sea: A 1- year survey. J. Geophys. Res. Oceans 111, C09010, 2006.

Bourne, M. D., A. L. Thomas, C. Mac Niocaill, and Henderson G. M.: Improved determination of marine sedimentation rates using 230Thxs, Geochem. Geophys. Geosyst. 13, Q09017, doi:10.1029/2012GC004295, 2006.

Bressac, M., and C. Guieu: Post-depositional processes: What really happens to new atmospheric iron in the ocean's surface?. Global biogeochemical cycles 27, 859-870, 2013.

Bressac, M., Guieu, C., Doxaran, D., Bourrin, F., Obolensky, G., and Grisoni, J. M.: A mesocosm experiment coupled with optical measurements to assess the fate and sinking of atmospheric particles in clear oligotrophic waters. Geo-Marine Letters *32*, 153-164, 2012.

Bressac M., T. Wagener, A. Tovar-Sanchez, N. Leblond, S.H.M. Jacquet, A. Dufour, C. Guieu. Processes driving the iron cycle in the Mediterranean Sea. 2020 (this issue).

Candy, I., Black, S., & Sellwood, B. W.: Quantifying time scales of pedogenic calcrete formation using U-series disequilibria. *Sedimentary Geology*, *170*(3-4), 177-187, 2004.

Censi, P., Mazzola, S., Sprovieri, M., Bonanno, A., Patti, B., Punturo, R., ... & Alonzo, G.: Rare earth elements distribution in seawater and suspended particulate of the Central Mediterranean Sea. Chemistry and Ecology, 20(5), 323-343, 2004.

Desboeufs, K.V., R. Losno, & J.L. Colin, Factors influencing aerosol solubility during cloud process, Atmos. Environ., 35, 3529-3537, 2001.

Desboeufs, K., Leblond, N., Wagener, T., Nguyen, E. B., and Guieu, C.: Chemical fate and settling of mineral dust in surface seawater after atmospheric deposition observed from dust seeding experiments in large mesocosms, Biogeosciences, 11, doi:10.5194/bg-11-5581-2014, 2014.

Desboeufs, K., A. Sofikitis, R. Losno, J.L. Colin, & P. Ausset: Trace metals dissolution and solubility from mineral particles, Chemosphere, 58, 195-203, 2005

Duce, R. A., & Tindale, N. W.: Atmospheric transport of iron and its deposition in the ocean. Limnol. Oceanogr., 36(8), 1715-1726, 1991.

5   Fu F., Desboeufs K., Tovar-Sánchez A., Bressac M., Triquet S., Doussin J-F, Giorio C., Dulac F. & Guieu C., Solubility and concentration of trace metals and nutrients in wet deposition and impact on their marine concentration during PEACETIME cruise in the Mediterranean Sea, in preparation, 2020 (this issue).

Gazeau F., Alliouane, S., Stolpe, C., Irisson, J.-O., Marro S., Dolan J., Blasco T., Uitz J., Dimier C., Grisoni J.-M., De Liège G., Hélias-Nunige S., Djaoudi K., Pulido-Villena E., Dinasquet J., Obernosterer I., Ridame C., & Guieu
10   C. Impact of dust enrichment on Mediterranean plankton communities under present and future conditions of pH and temperature: an overview, in preparation, 2020a (this issue).

Gazeau, F., Marañón, E., Van Wambeke, F., Alliouane, S., Stolpe, C., Blasco, T., Ridame, C., Pérez-Lorenzo, M., Engel, A., Zäncker, B. and Guieu, C.: Impact of dust enrichment on carbon budget and metabolism of Mediterranean plankton communities under present and future conditions of pH and temperature,
15   Biogeosciences, 2020b (this issue).

Gehlen, M., Beck, L., Calas, G., Flank, A. M., Van Bennekom, A. J., & Van Beusekom, J. E. E.: Unraveling the atomic structure of biogenic silica: evidence of the structural association of Al and Si in diatom frustules. Geochim. Cosmochim. Acta, 66(9), 1601-1609, 2002.

Gerringa, L. J. A., Slagter, H. A., Bown, J., van Haren, H., Laan, P., De Baar, H. J. W., & Rijkenberg, M. J. A.:
20   Dissolved Fe and Fe-binding organic ligands in the Mediterranean Sea–GEOTRACES G04. Mar. Chem., 194, 100-113, 2017.

Gdaniec, S., Roy-Barman, M., Foliot, L., Thil, F., Dapoigny, A., Burckel, P, A. Masque, P., Garcia-Orellana, J., Morth M. & Andersson, P. S.: Thorium and protactinium isotopes as tracers of marine particle fluxes and deep water circulation in the Mediterranean Sea. Mar. Chem. 199, 12-23, 2018.

25   Greaves, M. J., Statham, P. J., & Elderfield, H.: Rare earth element mobilization from marine atmospheric dust into seawater. Mar. Chem. 46, 255-260, 1994.

Greaves, M. J., Elderfield, H., & Sholkovitz, E. R.: Aeolian sources of rare earth elements to the Western Pacific Ocean. Mar. Chem. 68, 31-38, 1999.

Guieu, C., et al. Iron from a submarine source impacts the productive layer of the Western Tropical South Pacific
30   (WTSP). Sci. Rep. 8, 9075, 2018

Guieu, C., D'Ortenzio, F., Dulac, F., Taillandier, V., Doglioli, A., Petrenko, A., Barrillon, S., Mallet, M., Nabat, P., and Desboeufs, K.: Process studies at the air-sea interface after atmospheric deposition in the Mediterranean Sea: objectives and strategy of the PEACETIME oceanographic campaign (May–June 2017), Biogeosciences Discuss., in review, 2020 (this issue).

35   Guieu, C., Dulac, F., Desboeufs, K., Wagener, T., Pulido-Villena, E., Grisoni, J. M., ... & Nguyen, E. B.: Large clean mesocosms and simulated dust deposition: a new methodology to investigate responses of marine oligotrophic ecosystems to atmospheric inputs. Biogeosciences, 7, 2765-2784, 2010.

Guieu, C., Loÿe-Pilot, M. D., Benyahya, L., and Dufour, A.: Spatial variability of atmospheric fluxes of metals (Al, Fe, Cd, Zn and Pb) and phosphorus over the whole Mediterranean from a one-year monitoring experiment:
40   Biogeochemical implications, Mar. Chem., 120, 164-178, https://doi.org/10.1016/j.marchem.2009.02.004, 2010.

Guieu, C., Roy-Barman, M., Leblond, N., Jeandel, C., Souhaut, M., Le Cann, B., ... & Bournot, C.: Vertical particle flux in the northeast Atlantic Ocean (POMME experiment). Journal of Geophysical Research: Oceans, 110(C7), 2005.

Haley, B. A., Klinkhammer, G. P., & McManus, J.: Rare earth elements in pore waters of marine sediments. Geochim. Cosmochim. Acta, 68(6), 1265-1279, 2004.

Hayes, C. T., Rosen, J., McGee, D., & Boyle, E. A.: Thorium distributions in high-and low-dust regions and the significance for iron supply. Global Biogeochemical Cycles 31, 328-347, 2017.

Hsieh, Y. T., Henderson, G. M., & Thomas, A. L.: Combining seawater ^{232}Th and ^{230}Th concentrations to determine dust fluxes to the surface ocean. Earth Planet. Sci. Lett., 312(3-4), 280-290, 2011.

Jickells, T. D., An, Z. S., Andersen, K. K., Baker, A. R., Bergametti, G., Brooks, N., ... & Kawahata, H.: Global iron connections between desert dust, ocean biogeochemistry, and climate. Science 308, 67-71, 2005.

Koeppenkastrop, D., & Eric, H.: Sorption of rare-earth elements from seawater onto synthetic mineral particles: An experimental approach. Chem.Geol, 95(3-4), 251-263, 1992.

Lal, D.: The oceanic microcosm of particles. Science, 198(4321), 997-1009, 1977.

Li, Y. H., Burkhardt, L., Buchholtz, M., O'Hara, P., & Santschi, P. H: Partition of radiotracers between suspended particles and seawater. Geochim. Cosmochim. Acta, 48(10), 2011-2019, 1984.

Louis, J., Gazeau, F., & Guieu, C. : Atmospheric nutrients in seawater under current and high pCO2 conditions after Saharan dust deposition: Results from three tank experiments. Prog. Oceanogr., *163*, 40-49, 2018.

Loÿe-Pilot, M. D., & Martin, J. M.: Saharan dust input to the western Mediterranean: an eleven years record in Corsica. In The impact of desert dust across the Mediterranean (pp. 191-199). Springer, Dordrecht, 1996.

Mahowald, N. M., Hamilton, D. S., Mackey, K. R., Moore, J. K., Baker, A. R., Scanza, R. A., & Zhang, Y.: Aerosol trace metal leaching and impacts on marine microorganisms. Nature communications, 9, 1-15, 2018.

Marchandise, S., Robin, E., Ayrault, S., and Roy-Barman, M.: U–Th–REE–Hf bearing phases in Mediterranean Sea sediments: Implications for isotope systematics in the ocean. Geochim. Cosmochim. Acta, 131, 47-61, 2014.

Measures, C. I., & Vink, S.: On the use of dissolved aluminum in surface waters to estimate dust deposition to the ocean. Global Biogeochemical Cycles, 14(1), 317-327, 2000.

Mendez, J., Guieu, C., and Adkins, J.: Atmospheric input of manganese and iron to the ocean: Seawater dissolution experiments with Saharan and North American dusts. Marine Chemistry, 120, 34-43, 2010.

Millero, F.J.: Solubility of Fe_III in seawater. Earth Planet. Sci. Lett. 154, 323–329, 1998.

Paris, R., K. Desboeufs, P. Formenti, S. Nava, and C. Chou, Chemical characterisation of iron in Dust and Biomass burning aerosols during AMMA-SOP0/DABEX: implication on iron solubility, Atmos. Chem. Phys., 10, 4273-4282, doi:10.5194/acp-10-4273-2010, 2010.

Paris, R., Desboeufs K. and Journet, E., Variability of dust iron solubility in atmospheric waters: Investigation of the role of oxalate organic complexation, Atmos. Environ., 45, 6510-6517, 2011.

Pavia, F. J., Anderson, R. F., Winckler, G. and Fleisher, M. Q.: Atmospheric Dust Inputs, Iron Cycling, and Biogeochemical Connections in the South Pacific Ocean from Thorium Isotopes, Global Biogeochemical Cycles, doi:10.1029/2020GB006562, 2020.

Pham, M. K., La Rosa, J. J., Lee, S. H., Oregioni, B., & Povinec, P. P.: Deposition of Saharan dust in Monaco rain 2001–2002: radionuclides and elemental composition. Physica Scripta, 2005(T118), 14, 2005.

Prospero, J. M., Nees, R. T., & Uematsu, M.: Deposition rate of particulate and dissolved aluminum derived from Saharan dust in precipitation at Miami, Florida. J. Geophys. Res.: Atmospheres, 92(D12), 14723-14731, 1987.

Prudêncio, M. I., Dias, M. I., Waerenborgh, J. C., Ruiz, F., Trindade, M. J., Abad, M., ... & Gouveia, M. A.: Rare earth and other trace and major elemental distribution in a pedogenic calcrete profile (Slimene, NE Tunisia). *Catena*, *87*, 147-156, 2011.

Rolison, J. M., Middag, R., Stirling, C. H., Rijkenberg, M. J. A., & De Baar, H. J. W.: Zonal distribution of dissolved aluminium in the Mediterranean Sea. Marine Chemistry 177, 87-100, 2015.

Roy-Barman, M.: Modelling the effect of boundary scavenging on Thorium and Protactinium profiles in the ocean, Biogeosciences, 6, 3091-3107, 2009.

Roy-Barman, M., Chen, J.H., Wasserburg, G.J.: The sources and the fates of thorium. Earth Planet. Sci. Lett. 139, 351–363, 1996.

Roy-Barman, M., Coppola, L., Souhaut, M.. Thorium isotopes in the western Mediterranean Sea: An insight into the marine particle dynamics. Earth Planet. Sci. Lett. 196, 161–174. doi:10.1016/S0012-821X(01)00606-9, 2002.

Roy-Barman, M., Lemaître, C., Ayrault, S., Jeandel, C., Souhaut, M., Miquel, J.C. : The influence of particle composition on Thorium scavenging in the Mediterranean Sea. Earth Planet. Sci. Lett. 286, 526–534. doi:10.1016/j.epsl.2009.07.018, 2009.

Santschi, P. H., Murray, J. W., Baskaran, M., Benitez-Nelson, C. R., Guo, L. D., Hung, C. C., ... & Roy-Barman, M. : Thorium speciation in seawater. Mar. Chem., 100(3-4), 250-268, 2006.

Savenko, A. V. and Savenko, V. S.: Aluminum hydroxide's solubility and the forms of dissolved aluminum's occurrence in seawater. Oceanology 51, 231-234, 2011.

Szabo, B. J., Haynes Jr, C. V., & Maxwell, T. A.: Ages of Quaternary pluvial episodes determined by uranium-series and radiocarbon dating of lacustrine deposits of Eastern Sahara. Palaeogeography palaeoclimatology palaeoecology, 1995.

Tachikawa, K., Jeandel, C., Roy-Barman, M.: A new approach to the Nd residence time in the ocean: the role of atmospheric inputs. Earth Planet. Sci. Lett., 170, 433-446, 1999.

Tachikawa, K., Roy-Barman, M., Michard, A., Thouron, D., Yeghicheyan, D., & Jeandel, C.: Neodymium isotopes in the Mediterranean Sea: comparison between seawater and sediment signals. Geochim. Cosmochim. Acta, 68(14), 3095-3106, 2004.

Taylor, S. R. and McLennan, S. M.: The geochemical evolution of the continental crust. Reviews of Geophysics 33, 241-265, 1995.

Ternon, E., Guieu, C., Loÿe-Pilot, M. D., Leblond, N., Bosc, E., Gasser, B., Miquel, J. C., Martin, J.: The impact of Saharan dust on the particulate export in the water column of the North Western Mediterranean Sea, Biogeosci., 7, 809–826, https://doi.org/10.5194/bg-7-809-2010, 2010.

Twining, B. S., Rauschenberg, S., Morton, P. L., and Vogt, S.: Metal contents of phytoplankton and labile particulate material in the North Atlantic Ocean. Progr. Oceanogr. 137, 261-283, 2015.

van de Flierdt, T., Pahnke, K., Amakawa, H., Andersson, P., Basak, C., Coles, B., ... & Goldstein, S. L.: GEOTRACES intercalibration of neodymium isotopes and rare earth element concentrations in seawater and suspended particles. Part 1: reproducibility of results for the international intercomparison. Limnol. and Oceanogr.: Methods 10, 234-251, 2012.

Wagener, T., Guieu, C., & Leblond, N.: Effects of dust deposition on iron cycle in the surface Mediterranean Sea: results from a mesocosm seeding experiment. Biogeosciences Discussions, 7(2). 2010

Wagener, T., Pulido-Villena, E., & Guieu, C.: Dust iron dissolution in seawater: Results from a one-year time-series in the Mediterranean Sea. Geophys. Res. Lett., 35(16), 2008.

Witter A.E., Hutchins D.A., Butler A. & Luther III G.W.: Determination of conditional stability constants and kinetic constants for strong model Fe-binding ligands in seawater ». Mar. Chem. 69, 1–17, 2000.

Weisrock, A., Rousseau, L., Reyss, J. L., Falguères, C., Ghaleb, B., Bahain, J. J., ... & Pozzi, J. P.: Travertines of the
Moroccan Sahara northern border: morphological settings, U-series datings and palaeoclimatic indications.
Géomorphologie: relief, processus, environnement, (3), 153, 2008

Table 1: Maximum percentage of dissolution and percentage of scavenging

	Fe	error	Al	error	La	error	Ce	error	Pr	error	Nd	error	Sm	error	Eu	error	Gd	error	Tb	error	Dy	error	Ho	error	Er	error	Tm	error	Yb	error	Lu	error	Th_conc	Th_isot* (range)	Pa
Percentage of dissolution (%)																																			
TYR_D	0.01	0.01	0.56	0.05																															
TYR_G	0.02	0.02	0.82	0.27																															
ION_D	0.01	0.01	0.91	0.04	1.9	0.3	2.2	0.2	2.8	0.2	3.6	0.3	4.0	0.3	4.5	0.2	4.4	0.2	4.9	0.2	5.3	0.3	5.5	0.6	5.1	0.4	4.4	0.5	4.1	0.3	4.1	0.4	1.20 0.20	0.7 (0.64-0.73)	
ION_G	0.03	0.03	0.96	0.09	2.2	0.2	2.5	0.2	3.0	0.2	3.7	0.2	4.0	0.2	4.3	0.1	4.5	0.2	4.8	0.2	5.1	0.3	5.4	0.3	4.9	0.4	4.4	0.5	3.8	0.1	3.7	0.3	0.77 0.06	1.1 (1.0-1.2)	
FAST_D	0.10	0.04	1.09	0.08	1.8	0.1	2.3	0.2	3.0	0.3	3.7	0.3	4.2	0.4	4.7	0.5	5.7	0.6	5.4	0.6	5.6	0.6	5.6	0.6	5.3	0.7	4.5	0.7	4.1	0.5	4.1	0.5	1.19 0.03	0.1 (0-8)	< 6%
FAST_G	0.04	0.01	1.13	0.03	2.2	0.4	2.5	0.3	3.1	0.3	3.8	0.4	4.1	0.3	4.3	0.3	4.6	0.3	5.1	0.2	5.5	0.3	5.9	0.3	5.3	0.3	4.4	0.1	4.1	0.3	3.6	0.1	1.08 0.13	2.4 (1-7)	
Percentage of scavenging (%)																																			
ION_D 72h					14.2	8.3	10.6	6.9	20.5	6.0	21.4	6.2	21.7	6.2	19.9	5.1	13.9	4.7	12.0	6.8	7.3	4.3	4.0	5.7	1.4	4.8	-1.2	5.6	-0.3	5.2	0.1	3.8	43 4		
ION_G 72h					9.5	3.9	7.9	2.7	18.8	2.7	19.7	2.7	20.4	3.3	18.2	1.9	14.8	4.0	11.9	3.4	8.7	2.0	4.6	1.7	3.2	2.3	2.9	3.3	0.9	0.3	0.7	3.5	45 2		
FAST_D 72h					25.2	6.1	26.7	6.2	30.9	5.9	28.5	5.8	28.6	6.7	26.6	8.1	22.8	7.4	20.6	7.3	14.9	8.0	7.8	9.1	4.7	9.0	1.6	9.7	4.2	8.6	3.0	10.2	64 2		
FAST_D 96h					18.3	5.9	35.9	4.8	36.7	5.0	36.2	4.7	33.9	7.1	34.7	8.0	29.3	7.1	26.5	7.3	17.7	8.4	9.8	9.6	6.8	9.8	4.6	10.5	12.8	8.5	3.6	10.8	60 1		
FAST_G 96h					15.1	4.6	22.7	1.4	20.6	4.5	22.6	4.3	25.1	2.3	20.0	1.7	16.6	2.2	13.5	2.9	9.1	2.9	4.5	3.4	0.5	2.1	-1.4	3.5	-1.5	3.5	-7.3	5.3	72 4		

The percentage of dissolution is calculated according to equation 1, except for Th_{isot} which is based on equation 4. The percentage of scavenging is calculated according to equation 2. For ^{232}Th, we did not take samples D1-12h and D1-24h, because they were considered contaminated (section 3.4). Taking theses samples into account would not change qualitatively the main conclusions of the study on thorium.

Figure caption:

Figure 1: concentrations of total dissolved Fe and Al during the dust addition experiments

Figure 2: Concentrations of dissolved REE during the tank experiments~~.~~ a) ION station~~.~~ b) FAST station. Crosses correspond to samples collected before dust addition (t = 0).

Figure 3: Dissolved ^{232}Th during the ION and FAST experiments. Note the ~~scale brake to show~~ the 3 outliers (contaminated samples). Crosses correspond to samples collected before dust addition (t = 0).

Figure 4: Dissolved Pa during the FAST experiments. <mark>Error bars correspond to the analytical uncertainties.</mark> Crosses correspond to samples collected before dust addition (t = 0).

Figure 5: Average maximum ~~percentage of~~ dissolution and ~~percentage of~~ scavenging ~~of~~ REE. ~~(a) Percentage of dissolution as defined by equation 1. Percentage of scavenging as defined by equation 2.~~ For ~~purpose of~~ comparison, ~~percentage of~~ scavenging was calculated ~~only~~ with data at t=72h for both ION and FAST.

Figure 6: ^{230}Th/^{232}Th versus $1/^{232}$Th mixing diagram for ION (left) and FAST (right) experiments. Seawater data pooled by time since dust addition: blue dots: t = 0 h (no dust addition yet); red dots: t = 1-6 h; orange dots: t = 24-48 h; yellow dots: t = 72-96 h. Yellow dots between brackets fall above the scavenging line for an unknown reason. Green dots: particles in the sediment traps. Red arrow: preferential release of ^{230}Th.
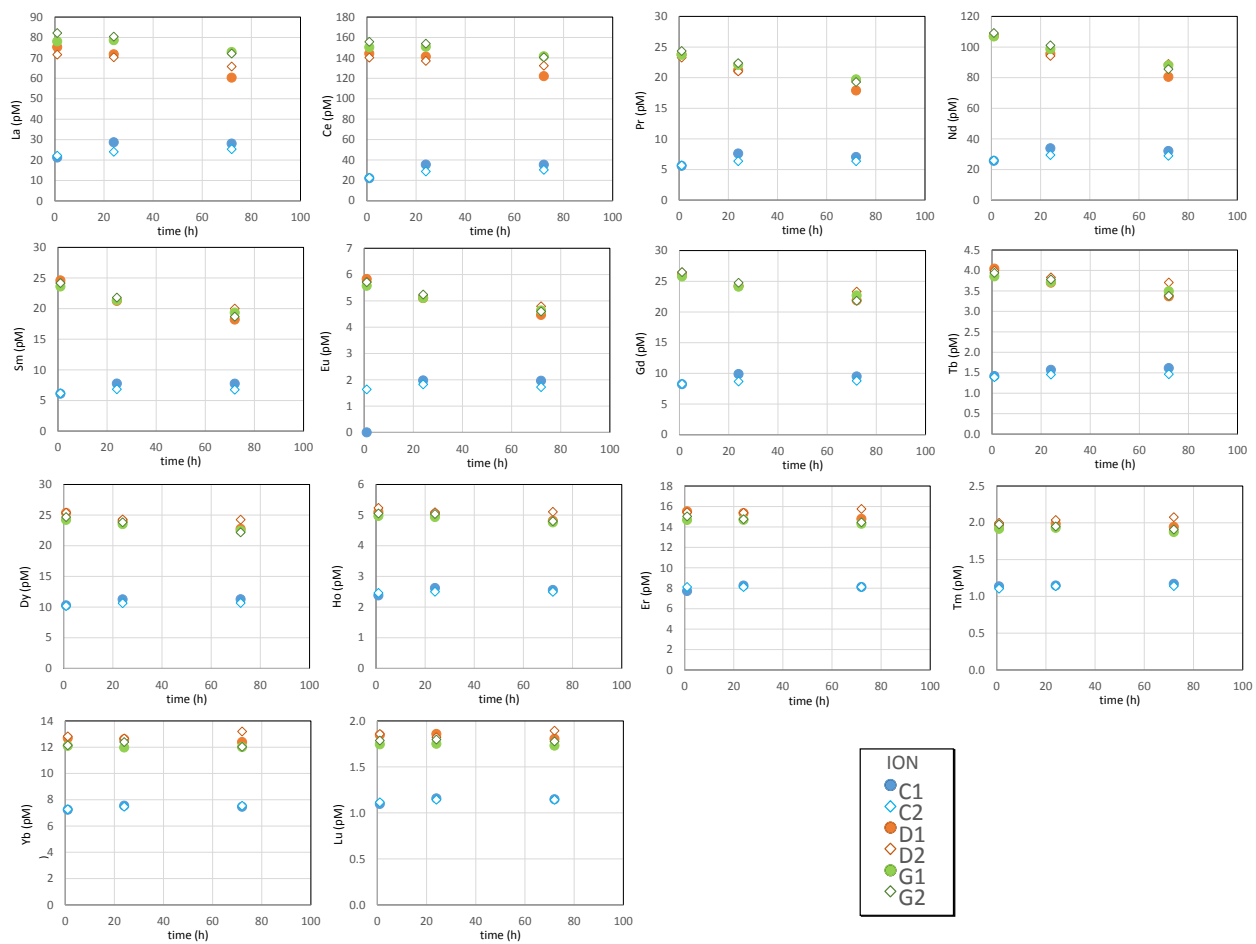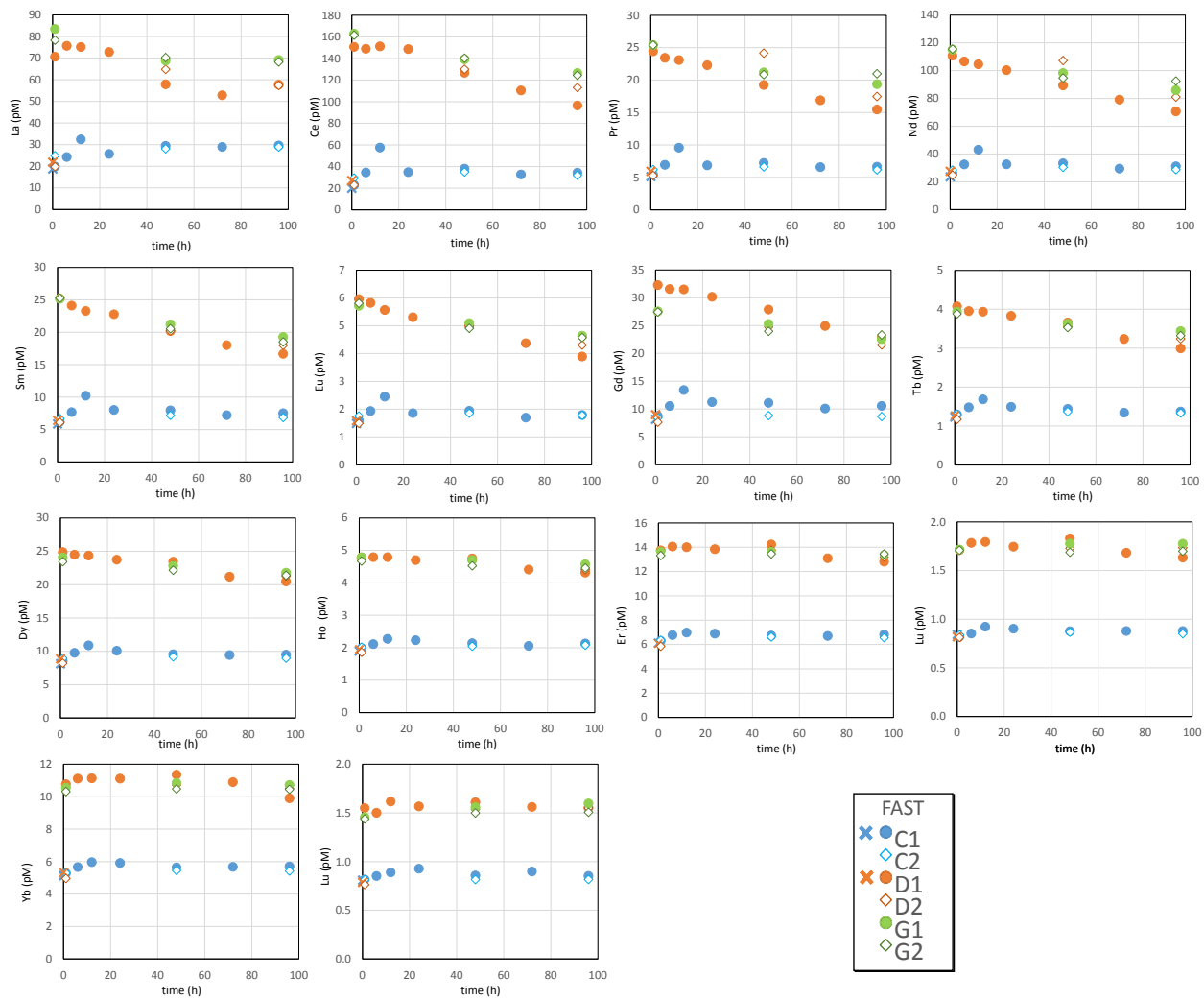
5

10   Fig 1

5

Fig 2a.

5

10

15   Fig 2b.
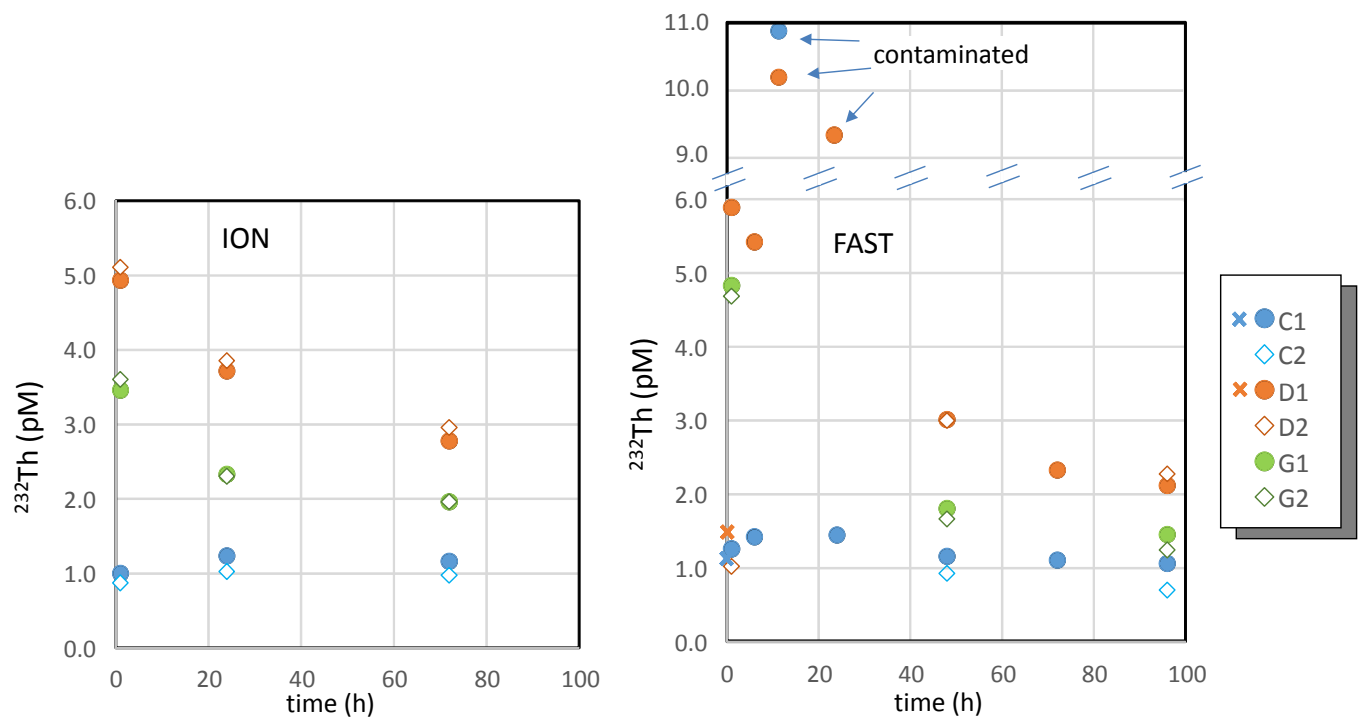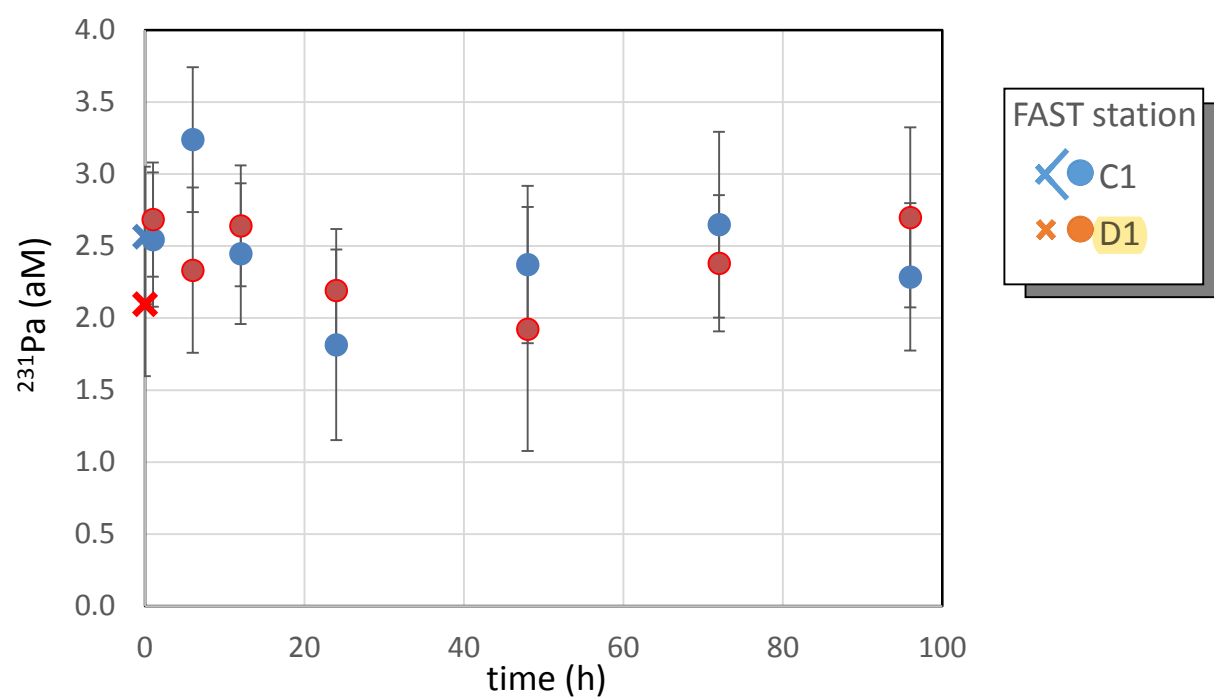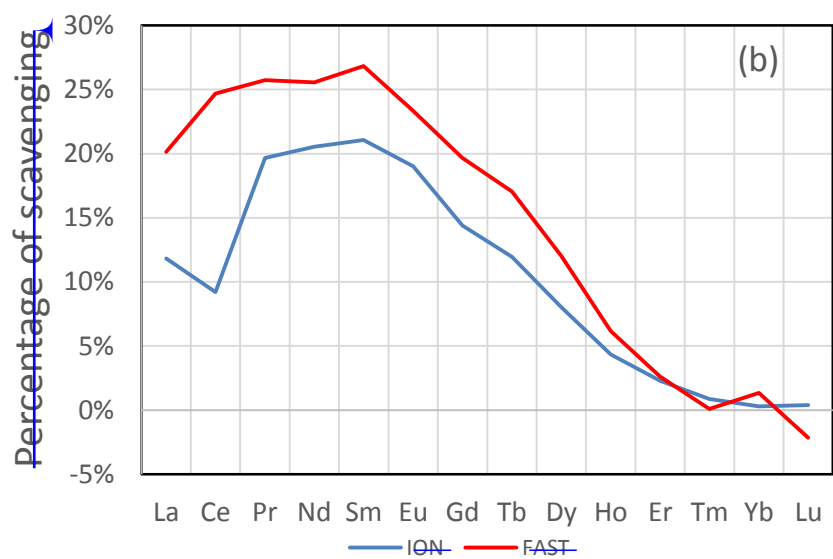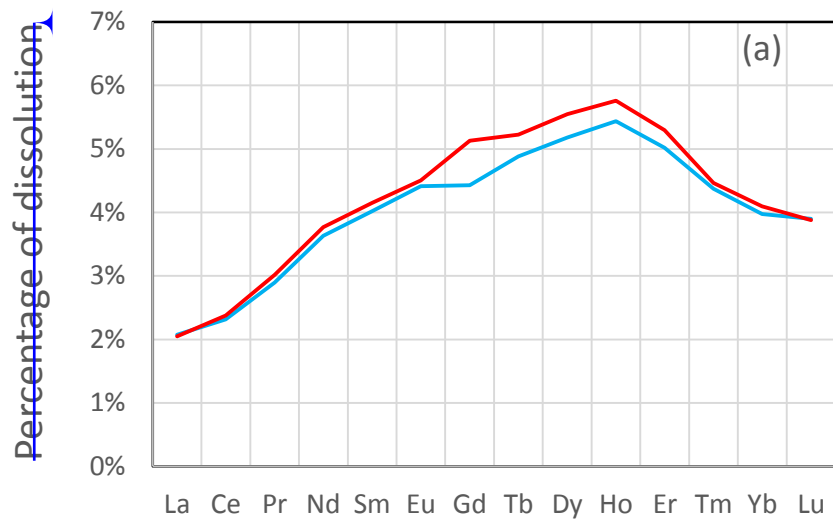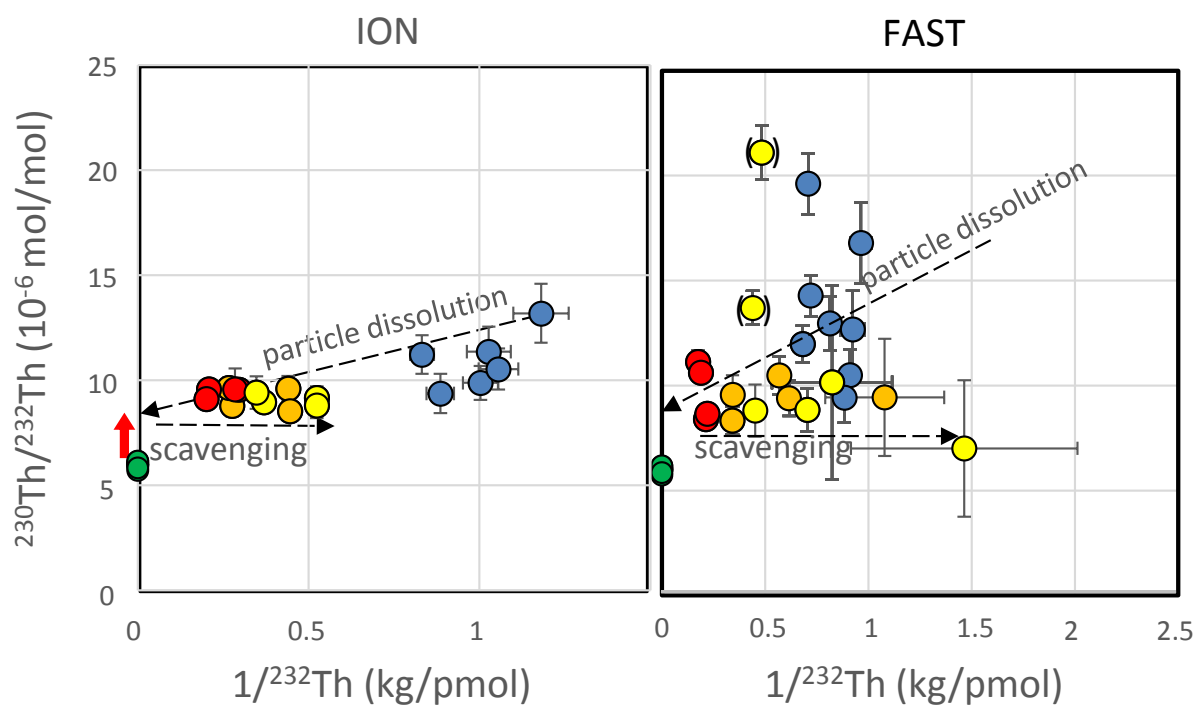
1

5

10

15

Fig. 3

2

5

10

15   Fig. 4:

Percentage of dissolution

(a)

La Ce Pr Nd Sm Eu Gd Tb Dy Ho Er Tm Yb Lu

Percentage of scavenging

(b)

La Ce Pr Nd Sm Eu Gd Tb Dy Ho Er Tm Yb Lu

ION   FAST

5

Fig. 5.

10

4

5

10

Fig. 6

15

Contrasted release of insoluble elements (Fe, Al, REE, Th, Pa) after dust deposition in seawater: a tank experiment approach

Matthieu Roy-Barman [1], Lorna Folio[1], Eric Douville[1], Nathalie Leblond[2], Frédéric Gazeau[3], Matthieu Bressac[3,4], Thibaut Wagener[5], Céline Ridame[6], Karine Desboeufs[7], Cécile Guieu[3]

Electronic Supplement

Tab. ES1: REE and Th GEOTRACES standard analyses

	light REE									medium REE											heavy REE											Thorium			
	La	2σ	Ce	2σ	Pr	2σ	Nd	2σ		Sm	2σ	Eu	2σ	Gd	2σ	Tb	2σ	Dy	2σ		Ho	2σ	Er	2σ	Tm	2σ	Yb	2σ	Lu	2σ		232Th	2σ	230Th	2σ
	(pM)		(pM)		(pM)		(pM)			(pM)		(pM)		(pM)		(pM)		(pM)			(pM)		(pM)		(pM)		(pM)		(pM)			(pM)		(aM)	
BATS 2000 m_1	17.9	0.47	5.37	0.2	3.84	0.12	17.2	0.5		3.56	0.2	0.89	0.05	4.9	0.2	0.76	0.03	5.55	0.2		1.41	0.1	4.66	0.2	0.69	0.02	4.5	0.2	0.72	0.03		113	160	37.3	1.1
BATS 2000 m_2	16.9	0.35	4.86	0.1	3.77	0.12	17.22	0.4		3.57	0.2	0.91	0.06	4.7	0.2	0.75	0.03	5.65	0.2		1.4	0.0	4.66	0.1	0.68	0.03	4.42	3.43	0.69	0.02		140	165	36.1	2.1
BATS 2000 m_3	16.4	0.84	4.94	0.2	3.72	0.13	16.96	0.5		3.58	0.2	0.89	0.04	4.5	0.2	0.76	0.03	5.5	0.2		1.36	0.1	4.62	0.2	0.64	0.04	4.33	0.48	0.69	0.05		126	171	37.8	0.9
average	17.1	1.08	5.06	0.4	3.77	0.08	17.12	0.2		3.57	0.02	0.9	0.01	4.7	0.3	0.76	0.01	5.57	0.1		1.39	0.0	4.65	0.04	0.67	0.04	4.41	0.12	0.7	0.03		126	19	37	1
consensual value	23		5.0		3.9		16.9			3.4		0.9		4.7		0.8		5.7			1.5		4.9		0.7		4.6		0.8			208		38	
	2.7		2.2		0.3		1.2			0.3		0.1		0.5		0.1		0.4			0.1		0.2		0.0		0.2		0.0			42		6	

5

Tab. ES2: Dissolved Fe and Al data

Station	tank	time	DFe	DAl	Station	tank	time	DFe	DAl	Station	tank	time	DFe	DAl
		(h)	(nM)	(nM)			(h)	(nM)	(nM)			(h)	(nM)	(nM)
TYR	C1	0	1.54	46.3	ION	C1	0	2.49	69.6	FAST	C1	0	1.73	24.1
	C1	24	1.11	47.4		C1	24	1.60	80.3		C1	24	1.34	23.5
	C1	72	1.60	47.8		C1	72	1.37	81.1		C1	72	0.88	27.4
	C2	0	1.53	50.3		C2	0	2.49	79.6		C2	0	1.94	24
	C2	24	0.67	42.8		C2	24	1.78	80.2		C2	24	1.80	23.5
	C2	72	1.41	46.1		C2	72	1.55	71		C2	72	0.99	27.7
	D1	0	1.46	43.9		D1	0	2.84	70.7		D1	0	6.68	49
	D1	24	1.45	79		D1	24	1.64	115.7		D1	24	2.66	61
	D1	72	1.35	102.2		D1	72	1.64	138.4		D1	96	9.69	107.4
	D2	0	1.61	44.1		D2	0	NA	70.7		D2	0	6.14	22.4
	D2	24	0.53	81.2		D2	24	1.52	113.4		D2	24	3.93	62.7
	D2	72	0.87	98.7		D2	72	1.36	135.6		D2	96	2.01	99.3
	G1	0	1.73	45.4		G1	0	5.10	83		G1	0	3.05	25.4
	G1	24	0.71	86.6		G1	24	2.52	112.7		G1	24	2.29	62.7
	G1	72	3.21	109.9		G1	72	3.53	136.4		G1	96	2.85	107.7
	G2	0	1.13	48.8		G2	0	2.04	79.3		G2	0	1.59	23.6
	G2	24	1.05	76		G2	24	1.53	112.5		G2	24	3.89	60.5
	G2	72	0.90	101.3		G2	72	1.45	144.2		G2	96	1.16	104.3

5

Tab. ES3: Dissolved REE, Th and Pa ~~data~~

tank	time (h)	La (pM)	2σ	Ce (pM)	2σ	Pr (pM)	2σ	Nd (pM)	2σ	Sm (pM)	2σ	Eu (pM)	2σ	Gd (pM)	2σ	Tb (pM)	2σ	Dy (pM)	2σ	Ho (pM)	2σ	Er (pM)	2σ	Tm (pM)	2σ	Yb (pM)	2σ	Lu (pM)	2σ	232Th (pM)	2σ	230Th (aM)	2σ	231Pa (aM)	2σ
		light REE								medium REE										heavy REE										Thorium				Protactinium	
ION C1	1	21	1	22	1	5.6	0.2	25.7	0.6	6.1	0.3	0.0	0.1	8.5	0.5	1.4	0.1	10.3	0.5	2.4	0.2	7.9	0.4	1.1	0.1	7.2	0.3	1.1	0.0	1.0	0.1	11.4	0.9		
ION C1	24	29	1	36	1	7.6	0.3	33.9	0.6	7.7	0.4	2.0	0.1	10.2	0.4	1.6	0.1	11.3	0.5	2.6	0.1	8.5	0.3	1.1	0.1	7.5	0.2	1.2	0.1	1.2	0.1	13.9	1.0		
ION C1	72	28	1	35	1	7.1	0.3	32.1	0.9	7.7	0.4	2.0	0.1	9.8	0.4	1.6	0.1	11.3	0.4	2.6	0.1	8.3	0.4	1.2	0.1	7.5	0.2	1.1	0.0	1.2	0.1	10.9	1.0		
ION C2	1	22	1	22	1	5.7	0.2	25.9	0.8	6.2	0.4	1.6	0.1	8.5	0.4	1.4	0.1	10.2	0.5	2.5	0.1	8.1	0.4	1.1	0.0	7.3	0.3	1.1	0.1	0.9	0.1	11.5	0.9		
ION C2	24	24	1	29	1	6.4	0.2	29.5	0.4	6.8	0.2	1.8	0.1	8.9	0.3	1.5	0.1	10.6	0.4	2.5	0.1	8.1	0.3	1.1	0.0	7.5	0.3	1.1	0.1	1.0	0.1	10.1	0.6		
ION C2	72	25	1	30	1	6.4	0.3	29.0	0.5	6.8	0.3	1.7	0.1	9.0	0.4	1.5	0.1	10.7	0.3	2.5	0.1	8.1	0.3	1.1	0.1	7.5	0.2	1.1	0.1	1.0	0.1	10.3	0.8		
ION D1	1	75	4	144	7	23.8	1.1	107.2	2.0	24.6	1.3	5.8	0.4	26.8	1.3	4.0	0.2	25.4	1.1	5.1	0.2	15.5	0.8	2.0	0.1	12.7	0.4	1.8	0.1	4.9	0.1	47.3	1.3		
ION D1	24	72	3	141	5	21.2	0.6	95.6	2.5	21.2	0.7	5.1	0.2	24.9	0.8	3.7	0.1	24.0	0.8	5.0	0.2	15.4	0.5	2.0	0.1	12.6	0.3	1.9	0.1	3.7	0.1	32.7	1.8		
ION D1	72	60	2	122	5	17.9	0.6	80.5	2.1	18.2	0.7	4.5	0.2	22.5	0.8	3.4	0.2	22.8	0.9	4.8	0.2	14.8	0.5	1.9	0.1	12.4	0.7	1.8	0.1	2.8	0.1	24.9	1.1		
ION D2	1	72	2	140	5	23.3	0.8	108.4	1.8	24.2	0.9	5.7	0.2	27.2	1.1	4.0	0.2	25.4	1.2	5.2	0.2	15.4	0.6	2.0	0.1	12.8	0.7	1.9	0.1	5.1	0.1	46.5	1.2		
ION D2	24	70	3	137	4	21.0	0.8	94.2	1.5	21.5	1.0	5.2	0.3	24.9	0.9	3.8	0.1	24.3	1.1	5.1	0.3	15.4	0.7	2.0	0.1	12.7	0.3	1.8	0.1	3.9	0.1	37.1	1.7		
ION D2	72	66	2	132	4	19.5	0.8	88.9	0.9	20.0	0.8	4.8	0.2	24.0	1.0	3.7	0.2	24.3	1.4	5.1	0.2	15.8	0.7	2.1	0.1	13.2	0.7	1.9	0.1	3.0	0.1	27.9	2.2		
ION G1	1	78	3	150	6	23.7	0.9	106.9	1.4	23.6	1.2	5.6	0.3	26.5	0.9	3.9	0.1	24.2	1.1	5.0	0.3	14.7	0.5	1.9	0.1	12.1	0.4	1.7	0.1	3.5	0.1	33.1	1.5		
ION G1	24	79	3	151	7	22.1	1.0	98.7	1.6	21.4	1.0	5.1	0.2	24.8	1.2	3.7	0.2	23.5	0.9	4.9	0.2	14.7	0.5	1.9	0.1	12.0	0.7	1.8	0.1	2.3	0.1	22.4	1.2		
ION G1	72	73	3	142	7	19.7	0.8	88.0	1.4	19.3	1.1	4.6	0.2	23.3	1.1	3.5	0.2	22.5	0.9	4.8	0.2	14.3	0.6	1.9	0.1	12.0	0.4	1.7	0.1	2.0	0.1	18.0	0.9		
ION G2	1	82	3	156	5	24.3	0.8	109.2	2.5	24.2	1.0	5.7	0.3	27.2	1.2	3.9	0.2	24.7	1.2	5.1	0.2	15.0	0.7	2.0	0.1	12.1	0.3	1.8	0.1	3.6	0.1	34.5	3.4		
ION G2	24	80	3	154	7	22.4	0.9	101.1	2.2	21.8	1.0	5.2	0.3	25.4	1.2	3.8	0.2	23.8	1.0	5.0	0.2	14.8	0.5	2.0	0.1	12.4	0.5	1.8	0.1	2.3	0.1	19.7	0.8		
ION G2	72	72	2	141	4	19.3	0.7	85.6	2.5	18.7	0.7	4.6	0.2	22.4	0.8	3.4	0.1	22.2	0.8	4.8	0.1	14.4	0.5	1.9	0.1	12.0	0.3	1.8	0.1	2.0	0.1	17.3	1.1		
FA C1	0	19	1	20	1	5.1	0.2	23.6	1.1	5.9	0.4	1.5	0.1	8.1	0.4	1.2	0.1	8.1	0.4	1.9	0.1	6.1	0.3	0.8	0.1	5.1	0.3	0.8	0.0	1.1	0.1	11.8	1.3	2.6	0.5
FA C1	1	20	1	23	1	5.4	0.2	26.1	1.0	6.2	0.4	1.6	0.1	8.7	0.4	1.3	0.1	8.6	0.4	2.0	0.1	6.3	0.3	0.8	0.1	5.3	0.2	0.8	0.1	1.3	0.1	16.4	1.5	2.6	0.5
FA C1	6	24	1	35	1	6.9	0.3	32.6	1.2	7.7	0.4	1.9	0.1	10.5	0.5	1.5	0.1	9.8	0.5	2.1	0.1	6.8	0.4	0.9	0.1	5.7	0.3	0.9	0.1	1.4	0.0	20.4	1.2	3.3	0.5
FA C1	12	32	1	58	3	9.6	0.4	43.1	1.8	10.2	0.5	2.5	0.1	13.4	0.6	1.7	0.1	10.9	0.5	2.3	0.1	7.0	0.3	0.9	0.0	6.0	0.2	0.9	0.0	10.9	0.1	94.7	2.5	2.5	0.5
FA C1	24	26	1	35	1	6.9	0.3	32.6	1.3	8.0	0.5	1.9	0.2	11.2	0.7	1.5	0.1	10.1	0.7	2.2	0.1	6.9	0.4	0.9	0.1	5.9	0.4	0.9	0.1	1.5	0.1	28.4	1.8	1.8	0.7
FA C1	48	29	1	38	2	7.2	0.3	33.3	1.3	8.0	0.4	1.9	0.1	11.1	0.6	1.4	0.1	9.6	0.5	2.1	0.1	6.7	0.4	0.9	0.1	5.6	0.2	0.9	0.1	1.2	0.1	10.9	1.3	2.4	0.5
FA C1	72	29	1	33	1	6.6	0.3	29.5	1.2	7.2	0.4	1.7	0.1	10.1	0.6	1.3	0.1	9.4	0.5	2.1	0.1	6.7	0.4	0.9	0.1	5.7	0.3	0.9	0.1	1.1	0.1	14.1	1.8	2.7	0.6
FA C1	96	30	1	34	1	6.7	0.3	31.2	1.2	7.5	0.5	1.8	0.1	10.6	0.6	1.4	0.1	9.5	0.5	2.1	0.1	6.8	0.4	0.9	0.1	5.7	0.3	0.9	0.1	1.1	0.1	17.9	1.8	2.3	0.5
FA C2	12	25	2	29	2	6.2	0.6	28.4	0.7	6.7	0.6	1.8	0.1	8.4	0.7	1.3	0.1	9	0.8	2.0	0.1	6.4	0.5	0.8	0.1	5.3	0.2	0.8	0.1	ND	ND	0.0	0.0		
FA C2	48	28	1	35	1	6.6	0.4	30.5	0.3	7.2	0.4	1.9	0.1	8.8	0.6	1.4	0.1	9	0.5	2.0	0.1	6.6	0.3	0.9	0.0	5.5	0.3	0.8	0.0	1.5	0.8	26.4	17		
FA C2	96	29	1	32	1	6.2	0.2	28.9	0.6	6.8	0.5	1.8	0.1	8.6	0.3	1.3	0.1	9	0.4	2.1	0.1	6.6	0.3	0.9	0.1	5.4	0.2	0.8	0.1	0.7	0.1	4.9	0.8		
FA D1	0	22	1	27	1	5.9	0.3	27.6	1.2	6.4	0.4	1.6	0.1	9.2	0.6	1.3	0.1	9	0.5	2.0	0.1	6.1	0.4	0.8	0.1	5.3	0.3	0.8	0.1	1.5	0.0	18.0	1.2	2.1	0.5
FA D1	1	71	3	151	6	24.4	1.0	110.8	4.0	25.2	1.0	6.0	0.3	33.1	1.4	4.1	0.2	25	1.0	4.8	0.2	13.7	0.6	1.7	0.1	10.8	0.4	1.5	0.1	5.9	0.1	65.5	3.0	2.7	0.4
FA D1	6	76	3	149	6	23.4	1.0	106.6	4.3	24.1	1.5	5.8	0.3	32.4	1.5	4.0	0.2	25	1.1	4.8	0.2	14.1	0.6	1.8	0.1	11.1	0.4	1.5	0.1	5.4	0.1	57.5	2.0	2.4	0.6
FA D1	12	75	2	151	6	23.1	0.9	104.6	4.1	23.3	1.1	5.6	0.3	32.3	1.7	3.9	0.2	24	1.4	4.8	0.3	14.0	0.9	1.8	0.1	11.1	0.7	1.6	0.1	10.2	0.1	85.4	2.4	2.7	0.4
FA D1	24	73	3	149	6	22.3	1.0	100.3	4.3	22.8	1.3	5.3	0.3	30.9	1.6	3.8	0.2	24	1.3	4.7	0.3	13.8	0.8	1.7	0.1	11.1	0.7	1.6	0.1	9.3	0.1	72.7	2.0	2.2	0.5
FA D1	48	58	3	127	6	19.2	0.8	89.4	3.7	20.2	1.1	5.0	0.2	28.6	1.3	3.7	0.2	23	1.1	4.8	0.2	14.2	0.7	1.8	0.1	11.4	0.4	1.6	0.1	3.0	0.1	25.1	1.9	2.0	0.8
FA D1	72	53	2	110	5	16.9	0.8	79.2	3.5	18.0	1.0	4.4	0.3	25.6	1.4	3.2	0.2	21	1.1	4.4	0.3	13.1	0.7	1.7	0.1	10.9	0.6	1.6	0.1	2.3	0.1	32.0	1.7	2.4	0.5
FA D1	96	58	2	97	3	15.5	0.6	70.7	2.7	16.7	1.1	3.9	0.3	23.4	1.4	3.0	0.2	20	1.3	4.3	0.3	12.8	0.8	1.6	0.1	9.9	0.6	1.6	0.1	2.1	0.1	44.8	2.4	2.7	0.6
FA D2	1	20	3	23	4	5.3	0.9	24.8	0.4	6.1	1.0	1.5	0.3	7.6	1.2	1.2	0.2	8	1.4	1.9	0.3	5.9	1.0	0.8	0.1	5.0	0.3	0.8	0.1	1.0	0.1	8.8	1.0		
FA D2	48	65	2	130	4	24.2	0.7	107.3	1.2	20.2	0.8	5.0	0.2	24.8	0.7	3.6	0.1	23	0.9	4.7	0.2	13.8	0.5	1.7	0.1	10.7	0.3	1.5	0.1	3.0	0.1	28.7	1.3		
FA D2	96	57	2	113	4	17.5	0.5	81.0	1.2	18.0	0.8	4.3	0.2	21.5	0.8	3.2	0.2	21	1.1	4.4	0.2	13.2	0.7	1.7	0.1	10.5	0.3	1.6	0.1	2.3	0.1	20.1	1.3		
FA G1	1	83	2	163	5	25.4	0.8	115.1	0.9	25.2	0.8	5.7	0.2	27.6	1.1	3.9	0.1	24	0.6	4.8	0.2	13.7	0.5	1.7	0.1	10.6	0.5	1.5	0.0	4.8	0.1	40.6	2.1		
FA G1	48	69	4	139	10	21.2	1.7	98.3	2.8	21.2	1.8	5.1	0.4	25.3	2.0	3.6	0.2	23	1.7	4.7	0.4	13.7	1.1	1.8	0.1	10.9	0.4	1.6	0.1	1.8	0.1	18.9	1.5		
FA G1	96	69	2	127	4	19.4	0.6	86.0	1.9	19.3	0.8	4.6	0.1	22.6	0.6	3.4	0.1	22	1.0	4.6	0.1	13.4	0.3	1.8	0.0	10.7	0.5	1.6	0.0	1.5	0.1	12.9	1.3		
FA G2	1	78	3	162	7	25.4	1.0	115.5	3.3	25.3	1.2	5.8	0.2	27.4	1.1	3.9	0.2	23	0.9	4.7	0.2	13.3	0.6	1.7	0.1	10.3	0.7	1.4	0.1	4.7	0.1	40.5	1.7		
FA G2	48	70	3	140	5	20.8	0.7	94.7	4.2	20.5	0.9	4.9	0.2	24.0	1.3	3.5	0.2	22	1.0	4.5	0.3	13.5	0.6	1.7	0.1	10.5	0.5	1.5	0.1	1.7	0.1	15.6	1.3		
FA G2	96	68	2	124	4	21.0	0.6	92.6	36	18.5	0.8	4.6	0.2	23.3	1.1	3.3	0.1	21	0.8	4.5	0.2	13.4	0.4	1.7	0.1	10.5	8.7	1.5	0.1	1.2	0.4	12.6	3.6		

5

Tab. ES4: ~~Major~~ elements in the sediment traps

Sample	sampling period	Particulate mass flux	POC fluxe	total Al flux	total Fe flux	BSi fluxe	BioFe flux	Delta Fe	BioAlFlux	deltaAl	fraction of seeded Al in the trap
-	day	mg/m2/d	mg/m2/d	mg/m2/d	mg/m2/d	mg/m2/d	mg/m2/d	nmol/L	mg/m2/d	nmol/L	
Tyr C1	3	0.8	0.3	ND	ND	ND	0.0001	0.01			
Tyr C2	3	1.5	0.5	ND	ND	ND	0.0003	0.02			
Tyr D1	3	1 704	21.1	85	45	31	0.0098	0.63	0.103	13.7	62%
Tyr D2	3	1 652	22.7	78	42	34	0.0106	0.68	0.113	15.1	57%
Tyr G1	3	1 841	24.4	87	48	40	0.0113	0.73	0.136	18.1	64%
Tyr G2	3	1 805	27.2	89	47	41	0.0126	0.82	0.139	18.5	65%
Ion C1	3	2.0	0.3	ND	ND	ND	0.0001	0.01			-
Ion C2	3	0.8	0.4	ND	ND	ND	0.0002	0.01			-
Ion D1	3	1 680	22.4	81	44	29	0.0104	0.67	0.097	13.0	59%
Ion D2	3	756	10.8	37	20	15	0.0050	0.32	0.052	6.9	27%
Ion G1	3	1 349	19.0	66	35	27	0.0089	0.57	0.091	12.2	48%
Ion G2	3	1 257	17.5	59	32	20	0.0081	0.52	0.067	8.9	43%
Fast C1	4	0.5	0.1	ND	ND	ND	0.0001	0.01			
Fast C2	4	1.0	0.2	ND	ND	ND	0.0001	0.01			
Fast D1	4	758	9.7	36	19	10	0.0045	0.39	0.035	6.2	35%
Fast D2	4	881	11.9	42	23	12	0.0056	0.48	0.040	7.2	41%
Fast G1	4	684	10.3	33	18	10	0.0048	0.41	0.033	6.0	32%
Fast G2	4	628	9.3	30	16	10	0.0043	0.37	0.035	6.2	29%

5   bio-Fe-flux calculated based on a Fe/C ratio of 100 µmol/mol. bio-Al-flux calculated based on a Al/Si ratio of 8000 µmol/mol.

10

Tab. ES5: Release ratio of trace elements relative to thorium (mol/mol).

	Fe/Th	Al/Th	error	La/Th	error	Ce/Th	error	Pr/Th	error	Nd/Th	error	Sm/Th	error	Eu/Th	error	Gd/Th	error	Tb/Th	error	Dy/Th	error	Ho/Th	error	Er/Th	error	Tm/Th	error	Yb/Th	error	Lu/Th	error	Pa/Th
ION_D	<200	17000	3000	13	3	29	6	4.4	0.8	20	4	4.5	0.8	1.0	0.2	4.5	0.8	0.6	0.1	3.7	0.7	0.7	0.1	1.8	0.3	0.2	0.0	1.3	0.2	0.18	0.03	<0.0001
ION_G	<874	28000	3400	23	3	50	5	7.1	0.7	32	3	6.8	0.7	1.5	0.1	7.1	0.7	1.0	0.1	5.5	0.5	1.0	0.1	2.6	0.3	0.3	0.0	1.9	0.2	0.25	0.03	
FAST_D	<1515	17200	1400	10	1	26	3	3.9	0.4	17	2	3.9	0.4	0.9	0.1	5.0	0.6	0.6	0.1	3.4	0.4	0.6	0.1	1.6	0.2	0.2	0.0	1.1	0.1	0.16	0.02	
FAST_G	<717	23000	2800	17	4	38	7	5.4	0.9	24	4	5.2	0.7	1.1	0.2	5.1	0.7	0.7	0.1	4.2	0.5	0.8	0.1	2.0	0.3	0.2	0.0	1.4	0.2	0.17	0.02	

Fig. ES1: Transect of the PEACETIME cruise. 10 short stations are numbered from St.1 to St.10. Stars named TYR, ION, and FAST indicate the 3 long stations where tank experiments were conducted.
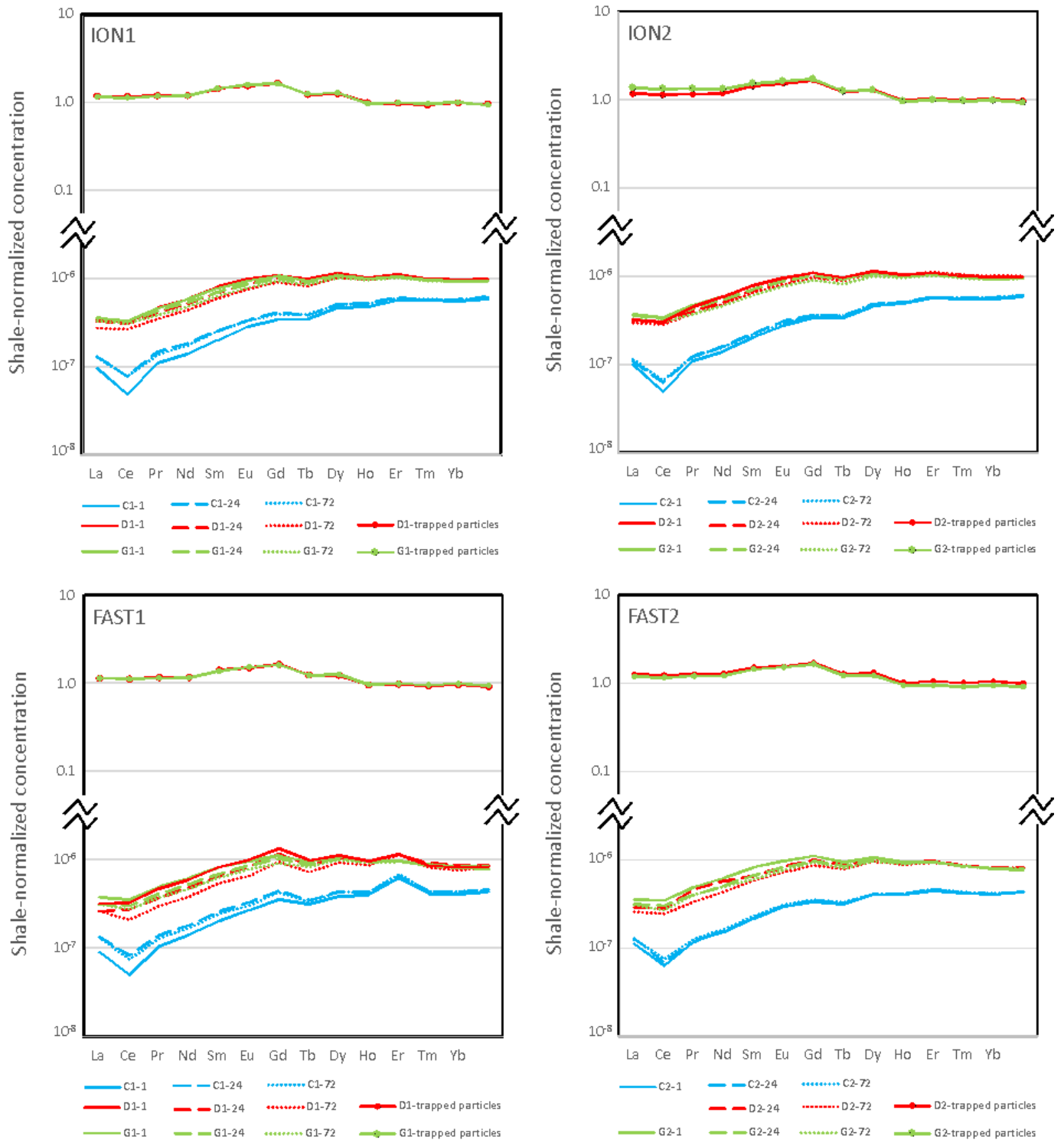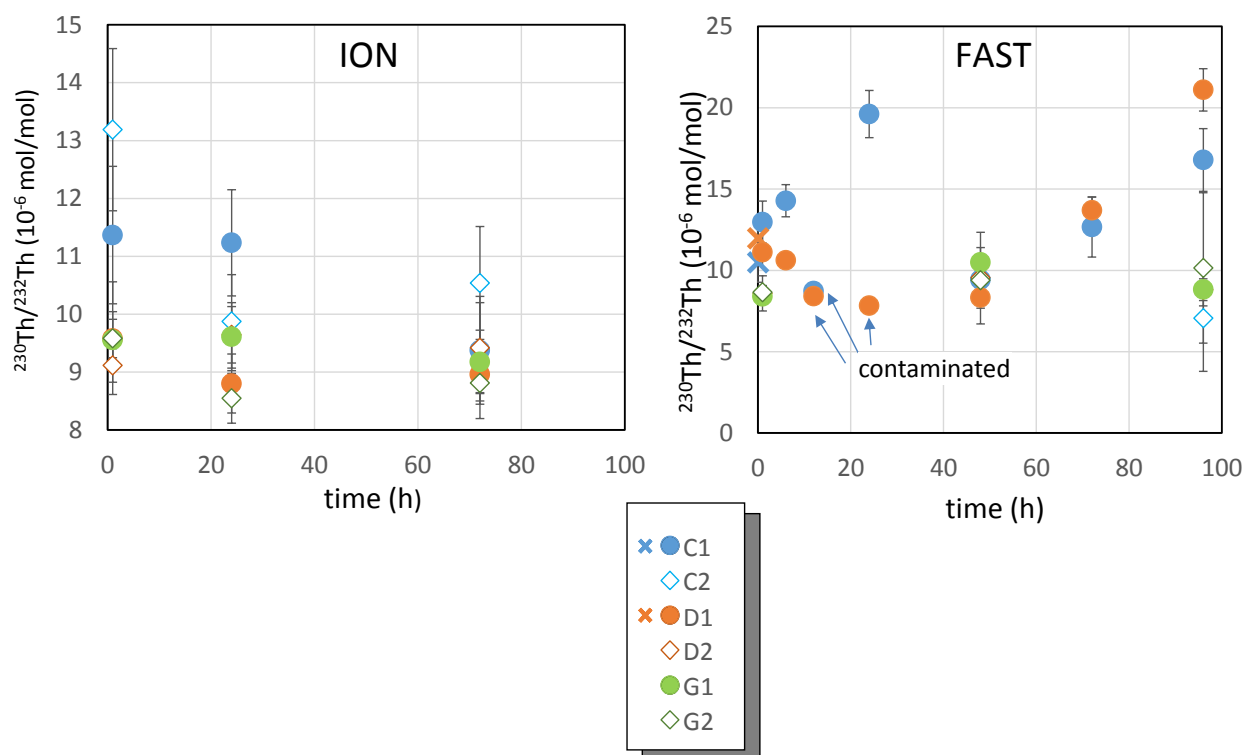
Fig. ES2: Shale-normalized concentrations of filtered seawater and ~~trapped particles~~. Note the scale break in the middle of the graph.

5

5

10

Fig. ES3: ^{230}Th/^{232}Th ratio during the tank experiments. a) ION station. b) FAST station. Crosses correspond to samples collected before dust addition (t = 0).

.